

INSPECTION AND EVALUATION OF AIR FILLED VOID INSIDE REINFORCED CONCRETE  
STRUCTURE BY NON-DESTRUCTIVE TESTING METHODS



A Thesis Submitted in Partial Fulfillment of the Requirements  
for the Degree of Master of Science in Earth Sciences

Department of Geology

FACULTY OF SCIENCE

Chulalongkorn University

Academic Year 2020

Copyright of Chulalongkorn University

การตรวจสอบและการประเมินโพรงอากาศภายในเนื้อคอนกรีตของโครงสร้างคอนกรีตเสริมเหล็กด้วย  
วิธีการตรวจสอบแบบไม่ทำลาย



วิทยานิพนธ์นี้เป็นส่วนหนึ่งของการศึกษาตามหลักสูตรปริญญาวิทยาศาสตรมหาบัณฑิต  
สาขาวิชาโลกศาสตร์ ภาควิชาธรณีวิทยา  
คณะวิทยาศาสตร์ จุฬาลงกรณ์มหาวิทยาลัย  
ปีการศึกษา 2563  
ลิขสิทธิ์ของจุฬาลงกรณ์มหาวิทยาลัย

Thesis Title	INSPECTION AND EVALUATION OF AIR FILLED VOID INSIDE REINFORCED CONCRETE STRUCTURE BY NON- DESTRUCTIVE TESTING METHODS
By	Mr. Thanakit Klomkiew
Field of Study	Earth Sciences
Thesis Advisor	Associate Professor Dr. Thanop Thitimakorn, Ph.D.

---

Accepted by the FACULTY OF SCIENCE, Chulalongkorn University in Partial  
Fulfillment of the Requirement for the Master of Science

----- Dean of the FACULTY OF SCIENCE  
(Professor Dr. POLKIT SANGVANICH, Ph.D.)

THESIS COMMITTEE

----- Chairman  
(Associate Professor Dr. SRILERT CHOTPANTARAT, Ph.D.)

----- Thesis Advisor  
(Associate Professor Dr. Thanop Thitimakorn, Ph.D.)

----- Examiner  
(Associate Professor Dr. SANTI PAILOPLEE, Ph.D.)

----- External Examiner  
(Assistant Professor Dr. Akkhapun Wannakomol, Ph.D.)

ธนภุต กลมเกลียว : การตรวจสอบและการประเมินโพรงอากาศภายในเนื้อคอนกรีต  
ของโครงสร้างคอนกรีตเสริมเหล็กด้วยวิธีการตรวจสอบแบบไม่ทำลาย. ( INSPECTION  
AND EVALUATION OF AIR FILLED VOID INSIDE REINFORCED CONCRETE  
STRUCTURE BY NON-DESTRUCTIVE TESTING METHODS) อ.ที่ปรึกษาหลัก : รศ.  
ดร.ฐานบ ธิติมากร

ปัจจุบันโครงสร้างส่วนใหญ่ในประเทศไทยเป็นโครงสร้างคอนกรีตเสริมเหล็ก เนื่องจากมี  
ความแข็งแรงและความทนทานต่อการเปลี่ยนแปลงสภาพแวดล้อม อย่างไรก็ตาม ความทนทาน  
ของคอนกรีตเกิดการเสื่อมสภาพได้ เพราะฉะนั้นการตรวจสอบคุณภาพคอนกรีตเพื่อซ่อมแซมและ  
บำรุงรักษาด้วยวิธีการที่เหมาะสมจึงสำคัญอย่างมาก ดังนั้นงานวิจัยนี้มีวัตถุประสงค์เพื่อทำการ  
ตรวจสอบข้อบกพร่องภายในโครงสร้างคอนกรีตเสริมเหล็ก โดยเฉพาะรอยแยกชั้นไม่ต่อเนื่องและ  
โพรงอากาศด้วยวิธีการตรวจสอบแบบไม่ทำลาย ประกอบด้วย 1)การสำรวจด้วยคลื่นอัลตราโซนิค  
แบบซีพजर 2)การสำรวจด้วยการสะท้อนของคลื่นอัลตราโซนิค 3)การสำรวจด้วยคลื่นความเค้น  
สะท้อน และ 4)การสำรวจด้วยคลื่นเรดาร์ โดยงานวิจัยนี้แบ่งออกเป็น 2 ส่วนหลัก ประกอบด้วย  
โครงสร้างอุดมคติจำลองข้อบกพร่องและโครงสร้างจริง การเปลี่ยนแปลงสัญญาณและพารามิเตอร์  
จากผลการทดสอบโครงสร้างอุดมคติ นำมาเป็นข้อแนะนำสำหรับทดสอบโครงสร้างจริงต่อไป และ  
สรุปยืนยันความถูกต้องจากวิธีการสุ่มเจาะเก็บตัวอย่างคอนกรีต

จากผลการศึกษาพบว่า ความแม่นยำ ความถูกต้อง ความเหมาะสม และประสิทธิภาพใน  
การตรวจสอบข้อบกพร่องจากการสำรวจด้วยคลื่นเรดาร์และการสำรวจด้วยคลื่นความเค้นสะท้อน  
ให้ผลลัพธ์ได้ดีกว่าวิธีอื่นๆ แม้ว่าวิธีการสำรวจด้วยคลื่นเรดาร์จะอ่อนไหวกับองค์ประกอบน้ำภายใน  
คอนกรีตที่มีอายุน้อยแต่วิธีการสำรวจด้วยคลื่นความเค้นสะท้อนไม่ได้รับผลกระทบดังกล่าว แต่การ  
สำรวจข้อบกพร่องในความเป็นจริงส่วนใหญ่ทดสอบที่อายุคอนกรีตมากกว่าช่วงการแข็งตัว  
นอกจากนั้น ขั้นตอนการเก็บข้อมูลและแปลผลของทั้ง 2 วิธี ใช้เวลาน้อยกว่าในพื้นที่ทดสอบ  
เดียวกัน

สาขาวิชา โลกศาสตร์  
ปีการศึกษา 2563

ลายมือชื่อนิสิต .....  
ลายมือชื่อ อ.ที่ปรึกษาหลัก .....

# # 6172179323 : MAJOR EARTH SCIENCES

KEYWORD: ground penetrating radar, ultrasonic pulse velocity, ultrasonic pulse echo, impact echo

Thanakit Klomkiew : INSPECTION AND EVALUATION OF AIR FILLED VOID INSIDE REINFORCED CONCRETE STRUCTURE BY NON-DESTRUCTIVE TESTING METHODS. Advisor: Assoc. Prof. Dr. Thanop Thitimakorn, Ph.D.

Nowadays, almost infrastructure in Thailand are almost reinforced concrete (RC) structure because they are strong and durable enough against environmental changes; nevertheless, the concrete durability will be decreased. The proper concrete integrity survey for potential remedy works is very importance, Thus, this research aims to inspect flaws especially delamination and air-filled void by four Non-Destructive Testing (NDT) methods be composed of 1) ultrasonic pulse velocity (UPV), 2) ultrasonic pulse echo (UPE), 3) impact echo (IE), and 4) ground penetrating radar (GPR). Furthermore, this research is separated two parts be consisted of idealized structures simulated defects and a realistic structure. The changing of signal patterns and parameters are performed on idealized structures along the hardening period is used for guidance to the realistic structure and verified an accuracy by core sampling method.

The research results are shown that the accuracy, precision, suitability, and performance of GPR and UPE method are better than the other methods. Although, the GPR method is sensitive with water content in an early concrete while the UPE method is not, the real case of flaw inspection is normally performed at an older concrete. Moreover, the data acquisition and interpretation of them were not used too much time in the same testing area.

Field of Study: Earth Sciences

Student's Signature .....

Academic Year: 2020

Advisor's Signature .....

## ACKNOWLEDGEMENTS

Firstly, I am heartfelt thanks to my parents for giving encouragement, enthusiasm, and invaluable assistance to me to be a better man. Without all of this, I might not be able to complete this research.

Secondly, I am really fortunate that I have a kind department manager of quality assurance, Mr. Natamon Kampananon, and project engineers, Mr. Chulaseth Krishnabhakdi and Mr. Napassapong Atthawit Jongjaiwanichkit, who give opportunities, suggestions, assistance, and guidelines to me to develop myself as I was studied a master degree at faculty of science, Chulalongkorn University. I also thank Thailand Science Research and Innovation (TSRI) to give opportunity and allow budgets support to support my research.

Thirdly, I would also like to thank Assoc.Prof. Thanop Thitimakorn, to be my kindly advisor who gives guidelines and encouragement to me, even my performance is not enough in some time.

Then, my completion of this project couldn't have been accomplished without the support of any technicians and coworkers from STS Corporation Co., ltd who help me prepare, check, and keep a lot of data that now complete interpretation and discussion in this research.

Finally, I apologize to all other unnamed who helped me in various ways to have good training.

Thanakit Klomkliew

## TABLE OF CONTENTS

	Page
.....	iii
ABSTRACT (THAI) .....	iii
.....	iv
ABSTRACT (ENGLISH) .....	iv
ACKNOWLEDGEMENTS .....	v
TABLE OF CONTENTS .....	vi
LIST OF TABLES .....	viii
LIST OF FIGURES.....	ix
CHAPTER 1 INTRODUCTION .....	1
1.1 Background and Significant of The Research .....	1
1.2 Problem Definitions.....	2
1.3 Research Hypothesis.....	2
1.4 Research Objectives.....	3
1.5 Research Scopes.....	3
1.6 Expected Outputs.....	3
1.7 Research Plan .....	3
CHAPTER 2 THEORIES AND LITERATURE REVIEWS.....	4
2.1 Deteriorations in Concrete Structure .....	4
2.2 Visual Inspection .....	7
2.3 Hammer Sounding.....	8
2.4 NDT Devices and Techniques for Concrete Structure .....	9

2.5 Related Researches .....	25
CHAPTER 3 RESEARCH METHODOLOGY .....	32
3.1 Searching for Theories and Literature Reviews .....	32
3.2 Searching for Civil Engineering Data and NDT Equipment .....	32
3.3 NDT on RC Mock-Up Simulated Defects Step .....	38
3.4 NDT on RC Structure Step .....	39
3.5 Interpretation, Analysis, and Discussion Step .....	40
3.6 Conclusion and Presentation Step .....	41
CHAPTER 4 RESEARCH RESULTS .....	42
4.1 Details of RC Mock-Up Simulated Defects .....	42
4.2 Results of NDT Signals on RC Mock-Ups .....	45
4.3 Realistic Structure in Research .....	61
4.4 Results of NDT signals on the Realistic Structure .....	63
CHAPTER 5 DISCUSSIONS AND CONCLUSIONS .....	69
5.1 Discussions .....	69
5.2 Conclusions .....	76
REFERENCES .....	78
VITA .....	83



## LIST OF TABLES

	Page
Table 1. Approximate impedances for different materials and reflection coefficient at interface were measured from a P-wave travelling through concrete.....	12
Table 2. Quality of concrete was classified from pulse velocity by UPV method.....	14
Table 3. Relative dielectric constants and radar wave velocity are resulted from pulse-transmitted through the material.....	24
Table 4. Simulated defect positions were concluded from four RC mock-up. ....	43
Table 5. The detectability of NDT methods over the hardening period were concluded from four RC mock-ups.....	60
Table 6. The detectability of NDT methods was descriptively compared with concrete cores.....	68
Table 7. Summary of Descriptive comparison of ranked lists. The detectability of NDT methods were descriptively compared with concrete cores.....	75

## LIST OF FIGURES

	Page
Figure 1. Heat-treating temperature effect on the concrete-compressive strength (Landkard et al., 1968).....	5
Figure 2. Schematic descriptive model of chemical damage level effect on the service life (Cusson et al., 2011).....	5
Figure 3. Distribution of seismic waves transmit through a homogenous material.....	10
Figure 4. Schematic illustrate the sign changes at interface from a) a concrete-air interface and b) a concrete-steel interface (Carino, 2015).....	13
Figure 5. Schematic illustrate a) the effects of defects on the travel time and b) the through-transmission test system of the ultrasonic pulse (ACI, 1998). ....	14
Figure 6. The typical configurations of the UPV method (Karaikos et al., 2015). ....	15
Figure 7. Schematic illustrate a) a pulse echo and b) a pitch catch of the UPE method (ACI, 1998).....	16
Figure 8. Possible scenario illustrate pulse reflection at different types of defection by using the UPE method (Stefan et al., 2018).....	17
Figure 9. Schematic of impact-echo method illustrate a) testing configuration, b) amplitude spectrum for test of solid slab, and c) amplitude spectrum for test over void in slab (ACI, 1998). ....	18
Figure 10. Significant vibration mode shapes of IE method are composed of a) Thickness mode and b) flexural mode (Carino, 2015).....	19
Figure 11. Typical signal results of IE method show a) time signal measured over the solid region, and over shallow delamination and b) frequency spectra corresponding to the two-time signals (Oh et al., 2013). ....	20
Figure 12. Signal results of IE method show a) time signal and b) frequency spectra corresponding to irregular wave fronts (Sansalone & Streett, 1997).....	20

Figure 13. Schematic show different effects of relative flaw size on the impact-echo response (Carino, 2015). .....	21
Figure 14. Three steps of the GPR method acquisition consist of a) schematic, b) received signal and graphic record output, and c) graphic recorder display a cross-sectional profile (ACI, 1998). .....	22
Figure 15. PROCEQ's PUNDIT Lab and 54 kHz transducers are performed for UPV method (www. proceq.com). .....	33
Figure 16. PROCEQ PUNDIT Live Array Pro wirelessly connect with tablet are performed for UPE method (www. proceq.com). .....	34
Figure 17. Impact Echo connect with tablet are performed for IE method (www.olsoninstruments.com). .....	35
Figure 18. PROCEQ GPR Live wireless connect with tablet for GPR method (www. proceq.com). .....	37
Figure 19. the cross sectional profile illustrate the resolution depth due to the ultra-wideband technology (www. proceq.com). .....	37
Figure 20. The designation of RC mock-up shows on plan and sectional views. ....	38
Figure 21. The example plan of realistic structure was illustrated crack lines on slab (Zoidis et al., 2013). .....	39
Figure 22. Flow chart exhibit 6 steps of research methodology. ....	41
Figure 23. Totally four RC mock-ups with simulated defects were constructed. ....	42
Figure 24. Plan views illustrate number of simulated defects from any mock ups composed of a) delamination, b) air-filled void, c) delamination and air-filled void, and d) unconsolidated concrete. ....	44
Figure 25. Four unconsolidated concretes illustrate the difference of void and concrete ratio by naked eyes. ....	45
Figure 26. Plan views illustrate line-scan testing patterns of a) GPR and b) UPE methods. ....	46

Figure 27. Line-scan testing over the hardening period was performed by GPR and UPE methods. ....	47
Figure 28. Selected a) GPR and b) UPE cross-sectional profiles on mock-up no.01 were compared results over hardening period with cross-section detail. ....	48
Figure 29. Selected a) GPR and b) UPE cross-sectional profiles on mock-up no.02 were compared results over hardening period with cross-section detail. ....	49
Figure 30. Selected a) GPR and b) UPE cross-sectional profiles on mock-up no.03 were compared results over hardening period with cross-section detail. ....	50
Figure 31. Selected a) GPR and b) UPE cross-sectional profiles on mock-up no.04 were compared results over hardening period with cross-section detail. ....	51
Figure 32. Plan views illustrate point testing patterns of a) IE and b) UPV methods. ...	52
Figure 33. Line-scan testing over the hardening period was performed by IE and UPV methods. ....	53
Figure 34. Exempler result of thickness frequency was inspected by IE method. ....	53
Figure 35. Example result of shifted frequency was inspected by IE method. ....	54
Figure 36. Example result of flexural frequency was inspected by IE method. ....	54
Figure 37. All NDT contour maps of mock-up no.01 were illustrated over hardening period. ....	55
Figure 38. All NDT contour maps of mock-up no.02 were illustrated over hardening period. ....	56
Figure 39. All NDT contour maps of mock-up no.03 were illustrated over hardening period. ....	58
Figure 40. All NDT contour maps of mock-up no.04 were illustrated over hardening period. ....	59
Figure 41. Overall realistic structure was inspected flaws in the research. ....	61
Figure 42. 1 <sup>st</sup> floor plan illustrates crack lines (red) and a testing area (green). ....	61

Figure 43. Example of crack width measurement was acquired by crack scale ruler on researching area. ....	62
Figure 44. Visual inspection and hammer sounding were performed on researching area and sectional detail of RC slab was illustrated.....	62
Figure 45. Plan view show testing patterns of a) IE and b) UPV methods. ....	63
Figure 46. Plan view show testing patterns of a) GPR and b) UPE methods. ....	63
Figure 47. Four NDT method were performed on a testing area.....	64
Figure 48. All NDT contour maps with selected coring positions (purple star) were illustrated on researching area. ....	65
Figure 49. Comparison between a) GPR and b) UPE profiles were only shown missing signal (green rectangular) on GPR profile at coring position no.01.....	66
Figure 50. Comparison between a) GPR and b) UPE profiles were shown significant signal (green rectangular) on UPE profile at coring position no.02. ....	66
Figure 51. Comparison between a) GPR and b) UPE profiles were shown significant signal (green rectangular) on UPE profile at coring position no.03. ....	66
Figure 52. Comparison between a) GPR and b) UPE profiles were shown significant signal (green rectangular) on UPE profile at coring position no.04. ....	66
Figure 53. Four concrete coring samples were shown concrete integrity and physical defects (red rectangle).....	67
Figure 54. UPV contour mappings from other research were illustrated the difference using of concrete quality criteria (Lorenzi et al., 2015). ....	70
Figure 55. UPV contour mapping results between a) other research and b) this research were compared. ....	70
Figure 56. IE contour mappings from other research were illustrated the different using of dominant criteria (Azari et al., 2014). ....	71
Figure 57. Different concrete thickness affect to dominant frequency (Azari et al., 2014). ....	71

Figure 58. IE contour mapping results between a) other research and b) this research were compared. ....	72
Figure 59. Example of UPE profiles show the profile results over delamination (left) and sound concrete (right) (Stefan et al., 2018).....	73
Figure 60. Example research result of a) UPE and b) GPR were illustrated by contour map. ....	73
Figure 61. Void thickness at the peak response as a function of material and frequency (David, 2017).....	74



## CHAPTER 1 INTRODUCTION

### 1.1 Background and Significant of The Research

The Reinforced Concrete (RC) structures in Thailand is the most compromised of a wide range of structure types, such as columns, beams, slabs, pavements, etc. and too many of them are aging. Thus, inspection, assessment and maintenance of the existing RC structures has been very important before rehabilitation. The most interesting of the inspection and assessment is concrete strength and some material properties but the integrity is recently be truly considered. The concrete integrity of RC structure is a major factor that influences loading capacity and life-building expectancy. Defected inspection especially air-filled void and delamination in concrete has always been a typical defect that may occur in the construction process, an accident from impact or fire, and corroded rebar occurrence while using the building. If the building has been detected at any points that is maybe at the joint or the vital point happens to certain large air-filled void or delamination, it could decrease structural stability and environmental durability of concrete material. Thus, precision and accuracy from the inspection and evaluation, such as dimension, position, and shape by non-destructive testing (NDT) methods are very important. These can lead to design the proper way for suitable remedy work, which can save cost and time in the maintenance process.

Nowadays, many NDT techniques require good contact between the tested concrete surface and the sensor of devices to obtain data. However, the concrete surface is rough or limited access due to the difference in building usage. Thus, the elimination of rough surfaces is necessary before doing the tests. However, some NDT methods need not eliminate the surface because it uses non-contact techniques such as penetrating radiation. The penetrating radiation uses electromagnetic (EM) pulse waves to detect the difference of the dielectric properties, such as rebars, defects, tendons, etc. in concrete by EM wave reflection on the testing profile. These

EM wave is disturbed by moisture and salts content within the concrete, thereby it complicates the interpretation for defect detection and identification. On the other hand, elastic wave test methods, composed of ultrasonic pulse velocity, ultrasonic pulse-echo, and impact echo, can inspect defects below the surface by the difference of elastic properties of materials, such as thickness, defects, crack depth and strength. However, the limitation of elastic wave methods requires smooth contact between the probes and the concrete surface for decreasing disturb of signals and reduce the efficiency of measurement.

Therefore, four NDT methods; consisting of impact echo (IE) method, ground-penetrating radar (GPR) method, ultrasonic pulse velocity (UPV) method, and ultrasonic pulse echo (UPE) method are used to inspect and evaluate the difference of dimensions, positions, and shapes of the delamination and air-filled void in this research. Last but not least, the research results are interpreted and then are compared in term of precision, accuracy, suitability, and performance with the actual level of the simulate defect and concrete core sampling method in the idealized structures and on the realistic structure, respectively.

### **1.2 Problem Definitions**

- 1) How do signal characteristics of different NDT methods change when they move through or reflect at different material properties of 7, 14, 28, and 56 concrete day life?
- 2) What NDT methods in the research are the best to inspect and evaluate defect positions by descriptive comparison?

### **1.3 Research Hypothesis**

The descriptive comparison results will be showed that the GPR and UPE method are more accurate and precise than the other NDT methods from both the idealized structure along with the difference of concrete day-life, hardening peroid, and the realistic structures.



#### 1.4 Research Objectives

- 1) To apply four NDT methods to inspect and evaluate the size, shape, and position of any important defects inside concrete structures.
- 2) To compare in terms of performance, suitability, accuracy, and precision of any NDT methods.

#### 1.5 Research Scopes

- 1) Create reinforcement concrete mock-up simulated defects that have different materials, sizes, shapes, dimensions, and elevations for comparing the results from any NDT method along with different concrete day-life.
- 2) Inspect defects in reinforcement concrete structure by NDT methods and then randomly verify the accuracy and precision of any NDT methods by concrete core sampling methods.
- 3) Concludes and suggests the testing and survey results; however, this research is not included conclusion and suggestion of remedy and maintenance work.

#### 1.6 Expected Outputs

- 1) Know the proper direction of evaluation, suitability, accuracy, and precision of four NDT methods in this research.
- 2) Know the changing of signal characteristic of NDT methods when they detect delamination and air-filled void in concrete structure along the hardening period.

#### 1.7 Research Plan

This research plan contains six steps consisting of 1) searching for theories and literature reviews, 2) searching for civil engineering data and NDT equipment's procedures, 3) testing on RC mock-up simulated defects, 4) testing on RC structure which have defects, 5) interpreting and analysis the data from both 3 and 4 steps, and 6) conclusion and presentation of the research.

## CHAPTER 2 THEORIES AND LITERATURE REVIEWS

### 2.1 Deteriorations in Concrete Structure

In the past, properties of good concrete which civil engineers must always be considering had been workability, strength, impact and abrasion resistance, chemical stability, and permeability but concrete durability was not interested enough. The concrete durability is a major property against aging, increased building loads, changing environmental conditions, and advanced deterioration. If it was decreased due to the environmental changes, it will be harmful to the RC structure. Thus, concrete deteriorations are an effect on concrete durable of the structure which can results from many reasons, both inside and outside of the concrete. From the previous research (Settrabut, 1997), the report demonstrated that the concrete deterioration of RC structure which leading to corrosion causing cover delamination and air-filled void can be classified into 3 main causes.

Firstly, physical deterioration always affects concrete in the hardening period or after final setting time from tension stress, such as overloading, impact, dry-wet deterioration, and dry shrinkage from the high-temperature environment and fire hazard. The best example which represents the physical damage causes is a fire hazard. Although the concrete property is fire and heat resistance, it cannot resist fire or an unusually high temperature for a long time. The results will decrease the strength of the matrix and stiffness by spalling and shrinkage from the dehydration process as shown in Figure 1.

Secondly, the harmful level from chemical deterioration which can affect the RC structure depends on the concrete condition and chemical reactions with concrete and rebar from the surrounding environment, especially chemical factory, and some places that high population and traffic jam. The chemical reaction in Thailand which always affect the durability of concrete is sulfate attack, chloride attack, carbonation, alkali-aggregate reaction, and rebar corrosion. The chemical components of previous

chemical reactions come from the surrounding environment, such as atmosphere hydrosphere, and lithosphere diffuse into concrete and then the chemical reaction will decrease the resistance between concrete and rebars. The result is the rebar will be lost corrode resistance, depassivation, and then turn into rust at the rebar surface and tension stress build-up concrete damages on the structure as shown in Figure 2.

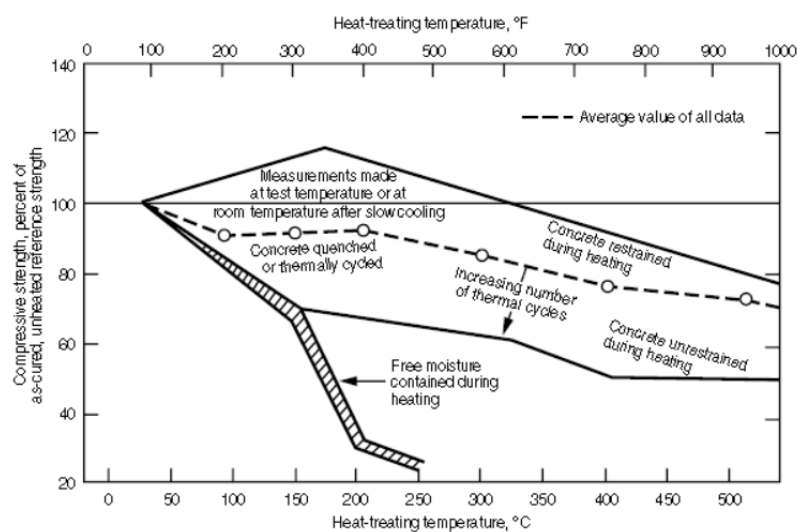


Figure 1. Heat-treating temperature effect on the concrete-compressive strength (Landkard et al., 1968).

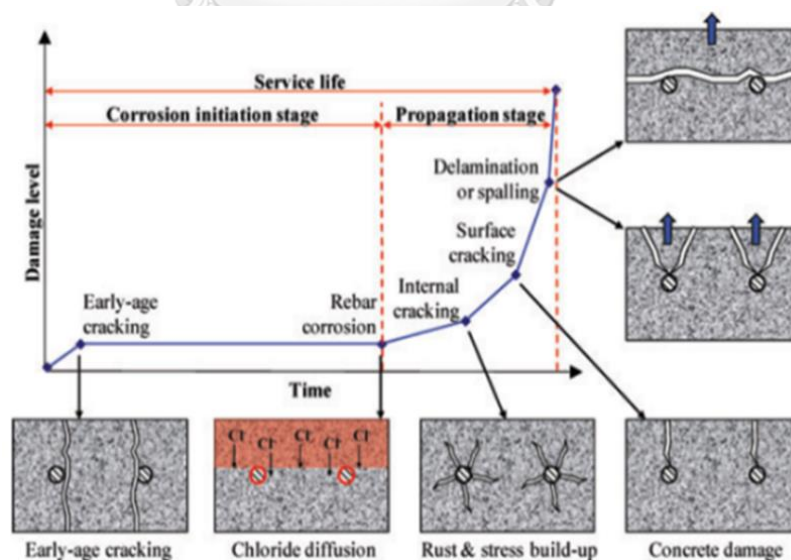


Figure 2. Schematic descriptive model of chemical damage level effect on the service life (Cusson et al., 2011).

Finally, mechanical deterioration is caused by abrasion at concrete surface, erosion from water and sand currents, and cavitation from the air bubble trapped in concrete. This mechanical damage cause is always found at traffic roads, bridges, underground structures, and failure from construction processes such as water-cement ratio, and other admixture designation are missed proportion.

However, the concrete damage can be an effect from a combination of factors that previously described, it will accelerate decrease the concrete durability and cause wider defects in the RC structures. The three common defects which influence from the previous deteriorations as described below.

- 1) Delamination is the most serious problem affecting the durability of the RC structures. The corrosion products increase the rebar volume by expansion and then the surrounding concrete will be disruptive stress. This defect type result is generally propagating in the planes of top rebar layers and parallel along the surface typically less than approximately 15 cm below.
- 2) Cracks are not only affecting a structure's severity but also reduces concrete durability. they can be caused by many reasons depend on surrounding factors. Moreover, they are a significant defect that can lead to failure of the RC structure by further accelerate the expansion rate. Determining the crack width and depth is important to the integrity assessment of the RC structure.
- 3) Voids and honeycombing are usually caused by poor consolidation of concrete during construction process, such as too fast to put casting out from concrete and not using vibrators while pouring. The size and position of air voids is depending on concrete component proportion and chemical admixtures. This defect type can appear at both concrete surface and deep of concrete surface, so the determination of them is important to the concrete integrity assessment of the RC structure.

## 2.2 Visual Inspection

The definition of visual inspection is structure survey by only eyesight with the equipment, such as a crack width scale ruler, and small hand-held magnifier by the qualified investigator. This inspection is the first step in the concrete integrity evaluation of the RC structure because it can previously identify the cause of observed distress and narrow down the critical areas in the structure. The standard documents refer from ACI 201.1R (ACI, 2008) which provide information for recognizing and classifying the different types of any defects and can identify the probable cause of the distress which are previously described. This suitable method typically involves the following patterns.

- 1) Gather information and background documents of the structure before walk-through inspection.
- 2) Plan and desire pattern of data acquisition for reference defects by making grid on surface of the concrete structure.
- 3) Record the survey data by the photograph and sketch the defect position on the investigation plan.

However, this method has the obvious limitation, it can be inspected only visible surfaces and the inspected results rely on inspector experience. Thus, internal defects, such as delamination and void are unnoticed. For these reasons, other NDT methods were performed to investigate the internal defects.

### 2.3 Hammer Sounding

The hammer sounding refer from ASTM D4580 (ASTM, 2003) is mainly used to detect shallow defects in the RC structures especially bridge and a wider range of structures. This method is often used for supporting the visual inspection for scoping the shallow defection area by transportation departments, the United States of America. This method can separate sound concrete area from the shallow defected area by hitting with a normal masonry hammer. The criteria for this method are ringing sound. If the testing area is sound concrete, the ringing sound is clear. On the other hand, the ringing sound is mute or hollow, the testing area has defected. The hollow sound is a result of the flexural oscillations of the shallow defects within the audible range. This suitable method typically involves the following patterns.

- 1) Preparing the areas by marking the grid point testing location and then hitting the hammer at any point.
- 2) Tapping around the concrete surface area that mute or hallow ringing sound for scoping area.
- 3) Record the survey data after complete testing and then drawing a contour map for interpretation.

In summary, this method is simple and rapid for acquisition and interpretation, but the results are subjective and vary from technician experience. Although this method is always used for bridge assessment, this research is desired to use it for supporting the visual inspection step.

## 2.4 NDT Devices and Techniques for Concrete Structure

The purposes of the NDT methods are used to determine concrete properties and evaluate the condition of the RC structure. The ACI committee 228.2 (ACI, 1998) concluded and provided eight NDT methods and techniques compose of 1) visual inspection, 2) stress-wave methods for structure, 3) stress-wave methods for deep foundation, 4) nuclear methods, 5) magnetic and electrical methods, 6) penetrability methods, 7) infrared thermography, and 8) radar method. Nevertheless, the research objectives and scopes concentrate on delamination and air-filled voids in the RC structure. Thus, only selected 2 NDT methods, exclude visual inspection, compose of the stress-wave method and the radar method are performed in this research.

### 2.4.1 Properties of stress waves

The pressure and deformation which suddenly apply on the surface of a solid can generate stress wave propagates through the solid. The speed of stress wave propagation is a function of the modulus of elasticity, the density, Poisson's ratio, and the geometry of solid. Thus, the characteristics of the tested solid depend on the properties of a solid and resultant of stress wave propagation permits. The stress wave propagates in a solid with a hemisphere wave fronts as two different waves composed of body waves, and surface waves as shown in Figure 3 below.

The body waves can separate as two sub-different waves include of P-wave and S-wave. The P-wave, compressional or dilatational wave, is associated with the propagation of normal stress and particle motion is parallel to the propagation direction. The S-wave, shear or transverse wave, is associated with shear stress and particle motion is perpendicular to the propagation direction. Another one of the surface waves is R wave, Rayleigh, which travels away from the pressure and deformation and then amplitude decreases exponentially along the surface.

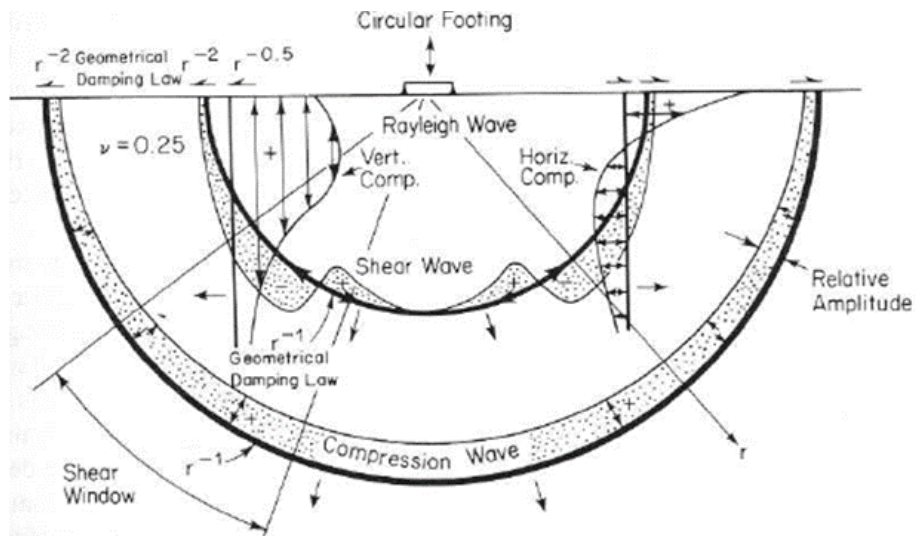


Figure 3. Distribution of seismic waves transmit through a homogenous material (Richart et al., 1970).

The NDT methods and techniques based on stress wave method is commonly used P-wave velocity ( $C_p$ ) and S-wave velocity ( $C_s$ ) for inspection, respectively. Due to the wave velocity depends on elastic constants and mass density of the solid which show in equations 1 and 2 below. Whereas  $\mu$ ,  $\lambda$  are Lamé's constants for solids, E is Young's modulus,  $\rho$  is density, and  $\nu$  is Poisson's ratio. From the equation 3, the  $C_s$  is slower than the  $C_p$  due to the S wave cannot propagate through the liquid phase. Thus, the ratio of  $C_s$  to  $C_p$  approximately equals 0.61 for a Poisson's ratio of 0.2, typically concrete. Moreover, the Rayleigh wave velocity ( $C_R$ ) is slightly slower than the shear wave velocity, due to the Poisson's ratio between 0.15 to 0.25. Thus, the ratio of  $C_R$  to  $C_s$  approximately equals 0.91 which show in equation 4 above.

$$C_p = \sqrt{\frac{\lambda+2\mu}{\rho}} = \sqrt{\frac{E(1-\nu)}{\rho(1-2\nu)(1+\nu)}} \dots\dots\dots (1)$$

$$C_s = \sqrt{\frac{\mu}{\rho}} = \sqrt{\frac{E}{2\rho(1+\nu)}} \dots\dots\dots (2)$$

$$\frac{C_s}{C_p} = \sqrt{\frac{1-2\nu}{2(1+\nu)}} \dots\dots\dots (3)$$



$$\frac{C_R}{C_S} = \frac{0.87+1.12\nu}{1+\nu} \dots\dots\dots (4)$$

Even though, the body wave velocity is seemed to greater than the surface wave velocity, the surface wave amplitude is larger. Therefore, the R waves are easily generated and readily sensed than the body waves. The advantage of the R wave is non-dispersive, and large distance detection because it out of plane motions compare with body wave. The limitation of the R wave is the limited penetration depth due to higher frequency from the impactor. However, the frequency can be decreased or increased by using the appropriate impact source.

From the previous paragraph, the stress wave methods and techniques can use for detecting the difference of materials in the layered media as RC structures by the interaction of reflected body waves at the interface between a dissimilar layer. Since the material has a unique specific acoustic impedance (Z) which is the product of the wave speed and density of the material. Therefore, the reflection (R) of body wave is a ratio of sound pressure of the reflected wave to the sound pressure of the incident wave which shows in equation 5 below. Whereas  $Z_2$  and  $Z_1$  are specific acoustic impedance of material 2 and 1, respectively.

$$R = \frac{Z_2-Z_1}{Z_2+Z_1} \dots\dots\dots (5)$$

Therefore, the NDT methods based on the stress-wave can detect defects in RC structure due to the reflection coefficient is closely 1.0 when finding an air interface. The following table shows approximate Z values for general materials (Sansalone & Carino, 1991)

Table 1. Approximate impedances for different materials and reflection coefficient at interface were measured from a P-wave travelling through concrete.

Material	Specification acoustic impedance, kg/(m <sup>2</sup> s)	Reflection coefficient at interface
Air	0.4	-1.00
Water	1.5x10 <sup>6</sup>	-0.65 to -0.75
Soil	0.3 to 4.0x10 <sup>6</sup>	-0.30 to -0.90
Concrete	7.0 to 10.0x10 <sup>6</sup>	-
Limestone	7.0 to 19.0x10 <sup>6</sup>	0.46
Granite	15.0 to 17.0x10 <sup>6</sup>	0.36 to 0.41
Steel	47.0x10 <sup>6</sup>	0.65-0.75

The reflection coefficient can be positive or negative depending on the relative values of the specific acoustic impedances of two materials which can be classified into 3 conditions (Sansalone & Streett, 1997). If  $Z_2$  is less than  $Z_1$ , such as a concrete-air interface, the reflection coefficient is negative which means the reverse the sign of incident wave, phase change. Thus, the incident wave with compressive stress would reflect as a tensile stress. If  $Z_2$  is greater than  $Z_1$  such as the concrete-rebar interface, the reflection coefficient is positive which means no change the sign of an incident wave. Thus, the incident wave with compressive stress would reflect as be the same. If  $Z_2$  is equal with  $Z_1$ , the incident wave will continue to pass through the materials. The P-wave changes sign at different interface from the condition above as shown in Figure 4 below. These different conditions are important criteria to precisely interpret and locate defects.

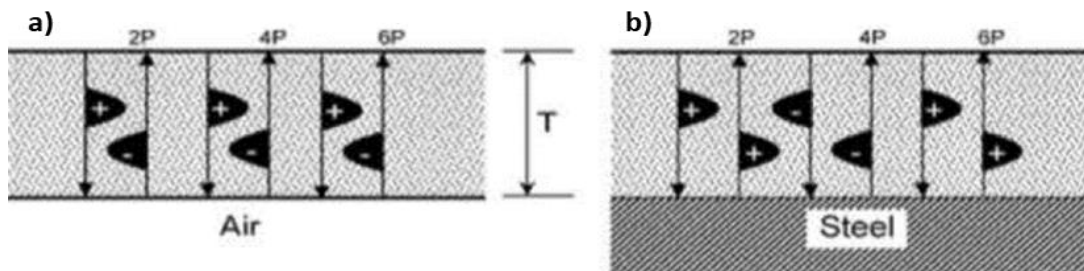


Figure 4. Schematic illustrate the sign changes at interface from a) a concrete-air interface and b) a concrete-steel interface (Carino, 2015).

#### 2.4.2 Stress wave-based NDT methods

The concrete structure inspection by the previous techniques has proven to locate defects because the large difference of  $Z$  between air and concrete can cause strong wave reflection at the interface layer, closely 1.0. The NDT techniques and methods base on stress wave propagation refer from ACI 228.2R (ACI, 1998) compose of ultrasonic through transmission method, ultrasonic-echo method, impact-echo method, and spectral analysis of surface waves. The research object is locating delamination and air-filled void in RC structures by body waves, therefore only 3 orders techniques and methods are used in the research.

##### 1) Ultrasonic through transmission / Ultrasonic pulse velocity (UPV) method

This technique is the oldest of the NDT method for determine crack depth (Zoidis et al., 2013) based on the stress wave propagation technique by measuring the travel time of a compressional wave over a known path length. Due to the  $C_p$  depends on the elastic constants and the mass density, it is possible to determine the uniformity or integrity of the concrete (Lorenzi et al., 2015). The testing principle is showed in Figure 5 below which represents different cases of ultrasonic pulses from one side to the other side. it shows that sound concrete results in the shortest travel time or fastest wave speed. In contrast, concrete with voids or cracks results in the longest travel time or slowest wave speed because of wave reflection from the air interface layer. The difference wave velocity from any points would locate the

defect areas or anomalies within the RC structures by classifying the level of concrete quality (Khan, 2002) in Table 2 below.

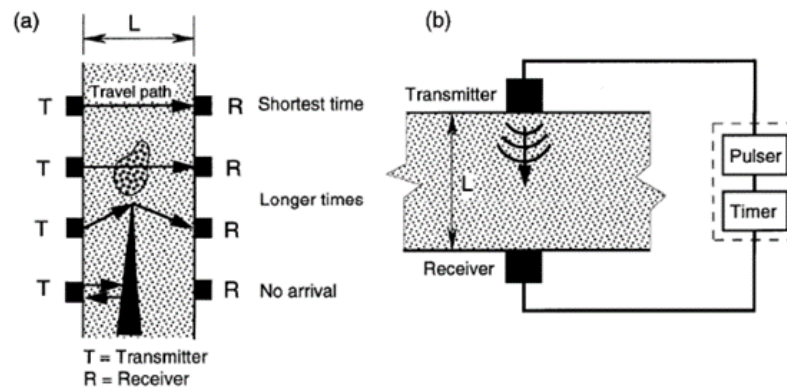


Figure 5. Schematic illustrate a) the effects of defects on the travel time and b) the through-transmission test system of the ultrasonic pulse (ACI, 1998).

Table 2. Quality of concrete was classified from pulse velocity by UPV method.

Longitudinal pulse velocity		Quality of concrete
Km/s. $10^3$	Ft/s	
>4.5	>15	Excellent
3.5 to 4.5	12 to 15	Good
3.0 to 3.5	10 to 12	Doubtful
2.0 to 3.0	7 to 10	Poor
<2.0	<7	Very poor

The components of measured devices composed of transmitting and receiving transducers and an accurate electronic timer refer to ASTM C597 (ASTM, 2002). The transducers have main 3 levels of resonant frequency, but the most common frequency which widely use is 40 kHz to 50 kHz for preliminary concrete condition survey (Nguyen & Modrak, 2018). Owing to testing areas in the RC structure surface is often rough, using gel or grease couplant before doing the test which obtains a stable result. After that, turning on the electronic timer, the signal pulse propagates from the transducer and then reflects another one at the opposite or similar side.

Besides, the UPV method can be set up an arrangement of the transducer in three typical configurations composed of a) direct transmission, b) semi-direct transmission, and c) indirect transmission show in Figure 6 below. The most common is the direct transmission mode but it is required access to both sides which suitable with columns, beams, and smaller testing areas. The indirect and semi-direct mode results between the travel time and the distance between transducers which could be an error from point shifting; however, they are required to assess only side or corner of the structure which suitable with slabs, walls, and wider testing areas.

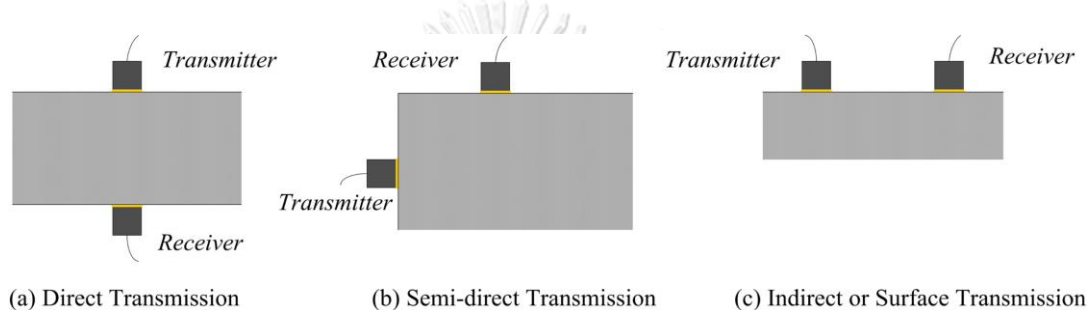


Figure 6. The typical configurations of the UPV method (Karaiskos et al., 2015).

The UPV method is a simple method for locating the defected area which have difference of concrete quality by creating the UPV contour mapping (Lorenzi et al., 2015). Nevertheless, the limitations of the UPV method need to access both sides of the structure surface, need smooth surface or using grease coupling for more accuracy, and cannot provide the depth of defects.

## 2) Ultrasonic pulse echo (UPE) method

This technique is early developed from the testing metals and then continuously adapted until development for the concrete structure measurement (Hoegh et al., 2011) and then concrete integrity (Stefan et al., 2018). The UPE method is not necessary to access both sides of the structure surface, due to access restriction or lack of information. The testing principle is showed in Figure 7 below which represents the wave propagation into the test object by transmitters. The wave propagates into the test objects and then is reflected or echoed by interface layers to the same transducers acting like a receiver. Thus, the travel time can be

determined from the transmitters to the receivers. the output is displayed on an oscilloscope as a time-domain waveform. Moreover, the accuracy of the UPE method for determining the depth of the reflecting interface layers is depended on knowing the wave speed of materials and the configuration of multiple-static array of transducers (Lybeart, 2017; Vonk & Taffe, 2018).

The components of measured devices composed of transmitting & receiving transducers, and an oscilloscope. It has been developed and applied to the concrete structures by using high frequency, 40 to 50 kHz, transducer as both the source and transducers. After the acquisition step, the data be processed and display the results as a cross-sectional profile, time-domain vs distance, on the display screen. If the testing position has defects such as voids, honeycomb, and microcracking in the RC structure, the cross-sectional profile shows the reflection or random scattering above the level of thickness along the scan line as shown in Figure 8.

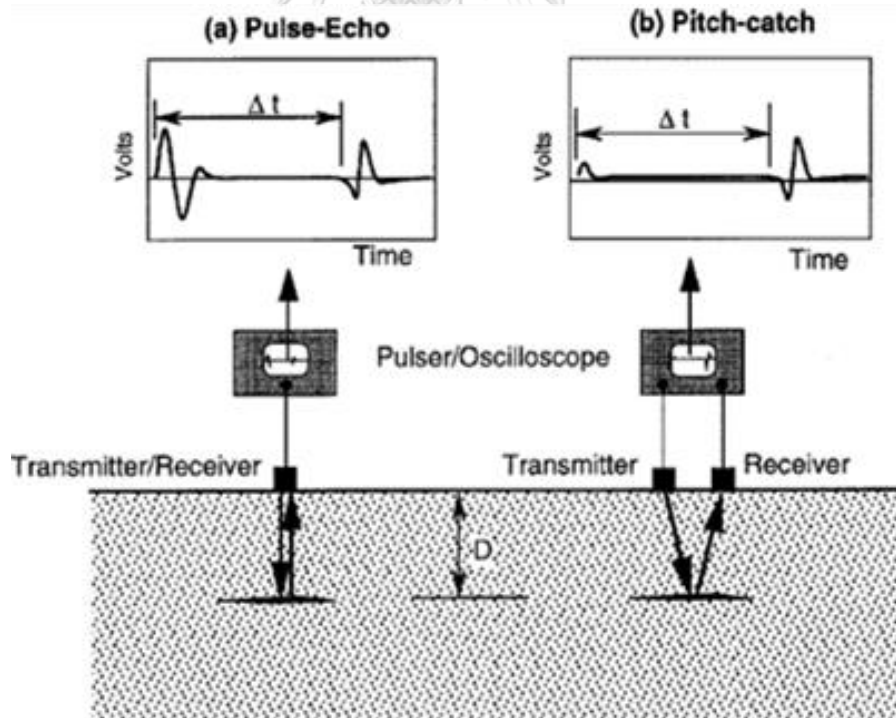


Figure 7. Schematic illustrate a) a pulse echo and b) a pitch catch of the UPE method (ACI, 1998).

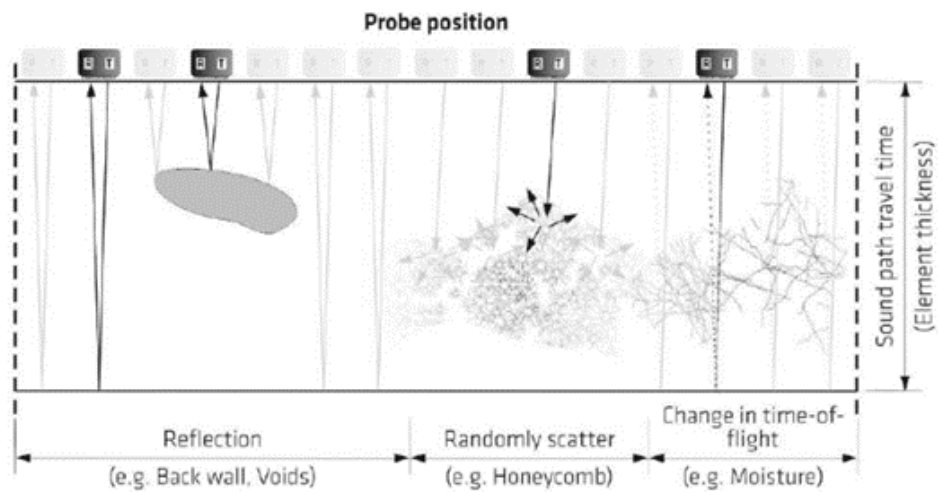


Figure 8. Possible scenario illustrate pulse reflection at different types of deflection by using the UPE method (Stefan et al., 2018).

The UPE method is a higher resolution of improved defects in RC structures than the UPV method. Nevertheless, the limitations of the UPE method are penetrating depth due to using high frequency and not have a worldwide standard.

### 3) Impact echo (IE) method

This technique is an old method and technique which generates a stress pulse by the short-duration mechanical impact on the concrete surface and then monitors the surface displacement by a transducer. At an early age, this method is widely used for evaluation of concrete pile and foundation and then continuously developed for evaluation of the concrete structure (Clausen et al., 2012) such as concrete thickness (Zoidis et al., 2013) and concrete integrity (Andrzej & Marta, 2014).

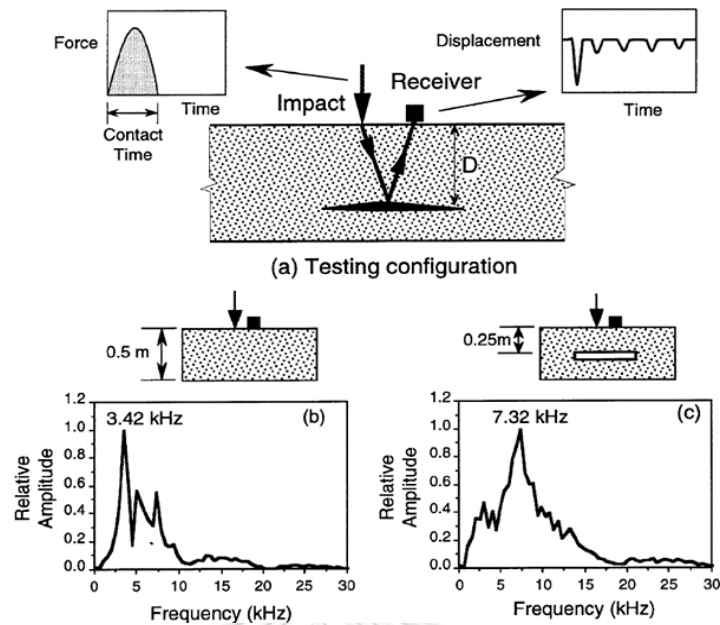


Figure 9. Schematic of impact-echo method illustrate a) testing configuration, b) amplitude spectrum for test of solid slab, and c) amplitude spectrum for test over void in slab (ACI, 1998).

The testing principle is showed in the previous Figure 9 a) which represents the wave propagation into the test object by the mechanical impact on the concrete surface. The body wave propagates into the test objects like a hemispherical wave front and the surface wave travels away from the impact point along the surface as shown in Figure 3. The body waves are reflected by internal interfaces or external boundaries. The receiving transducer measures the wave fronts displacement and records in the time domain using a data acquisition system. However, the interpretation of waveforms in the time domain for both thin and thick structural members is feasible, the interpretation by frequency analysis recommends a preferred approach. The frequency-domain transforms the time-domain signal by the fast Fourier transform technique and results in an amplitude spectrum. The principle of the frequency analysis concentrates on multiple reflections between the surface and reflecting interface. The thickness frequency, the peak amplitude spectrum, depends on the input parameter composes of the  $C_p$  and the distance ( $D$ ) between the reflecting interface and the test surface as shown in equation 6 below.



$$D = \frac{C_P}{2f} \dots\dots\dots (6)$$

The peak of the amplitude spectrum can be shifted when different interfaces are found in the structural member like Figure 9b) and 9c). The peak at 3.42 kHz corresponds to the thickness frequency of a solid slab while the shifted peak at 7.32 kHz corresponds to the frequency of interface within the solid slab such as void, honeycomb, and delamination.

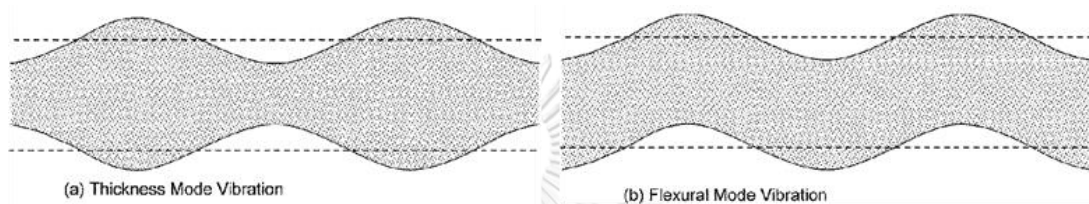


**Figure 10. Significant vibration mode shapes of IE method are composed of a) Thickness mode and b) flexural mode (Carino, 2015).**

Moreover, a specific vibration mode shape (Carino, 2015) is another criterion in defect detection, especially delamination. Due to the multiple reflections of P-wave make a resonance condition or frequency which striking a wine glass related to the geometry of the glass. The resonance frequency is associated with a specific vibration mode shape which found 2 general mode shapes as shown in Figure 10. The symmetrical mode shape in Figure 10a) is associated with a thickness mode frequency which represents the mid-plane of the plate. The other mode is anti-symmetrical mode shape due to opposite faces move in the same direction and is associated with a flexural mode vibration. The flexural mode vibration associate with shallow defect, depth less than 100 cm, or delamination because the resonant frequency is less than the structural thickness. Thus, the peak frequency of the flexural mode is shifted less than thickness frequency corresponding to the time signals as shown in Figure 11.

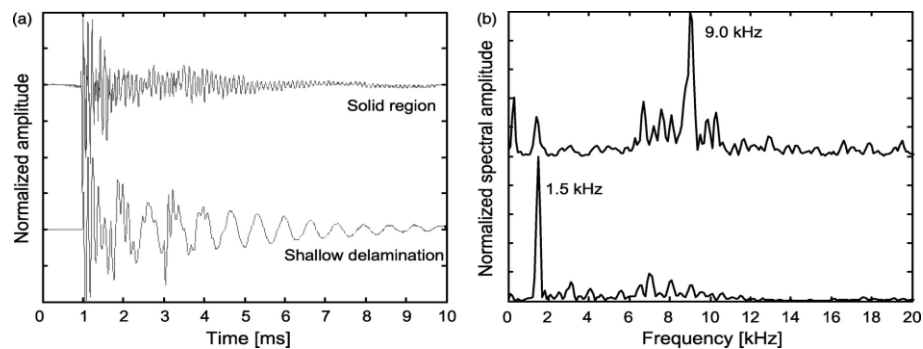


Figure 11. Typical signal results of IE method show a) time signal measured over the solid region, and over shallow delamination and b) frequency spectra corresponding to the two-time signals (Oh et al., 2013).

The other one of the defects that the research focus is unconsolidated concrete or honeycomb. The specific vibration mode of this defect is like thickness mode vibration; however, the result is dissimilar because of irregular wave fronts as shown in Figure 12 below. On the other hand, the unconsolidated concrete in real world may or may not be detected which depending on bubble size in the concrete structure due to the scattering of elastic waves (Stefan et al., 2018).

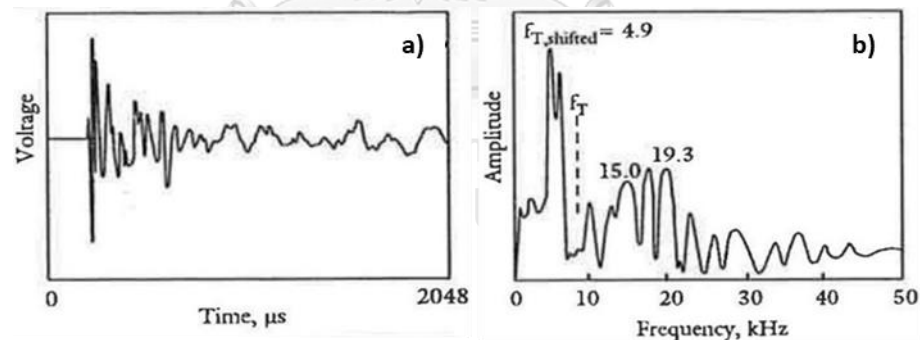


Figure 12. Signal results of IE method show a) time signal and b) frequency spectra corresponding to irregular wave fronts (Sansalone & Streett, 1997).

The difference in the peak frequency and the vibration mode shape obtained from any gridding points on the concrete surface can be analyzed with computer software. The analyzed results show as a cross-sectional view at any points and then it can be plotted on contour map which shows the difference of the peak frequency for comparison to other methods (Azari et al., 2014).

The components of measured devices composed of an impact source, a receiving transducer, and a data acquisition system refer to ASTM C1383 (ASTM, 1998). The impact source is a key success of the impact echo method due to the difference in impact duration determines the difference of frequency content which suitable for testing different structure member sizes. If the impact duration is shortened, high-frequency components are generated for evaluating the structural members less than 1 m thick. If the impact duration is lengthened, low-frequency components are generated for evaluating the structural members greater than 1 m thick. The transducer of the impact-echo method must use small accelerometers.

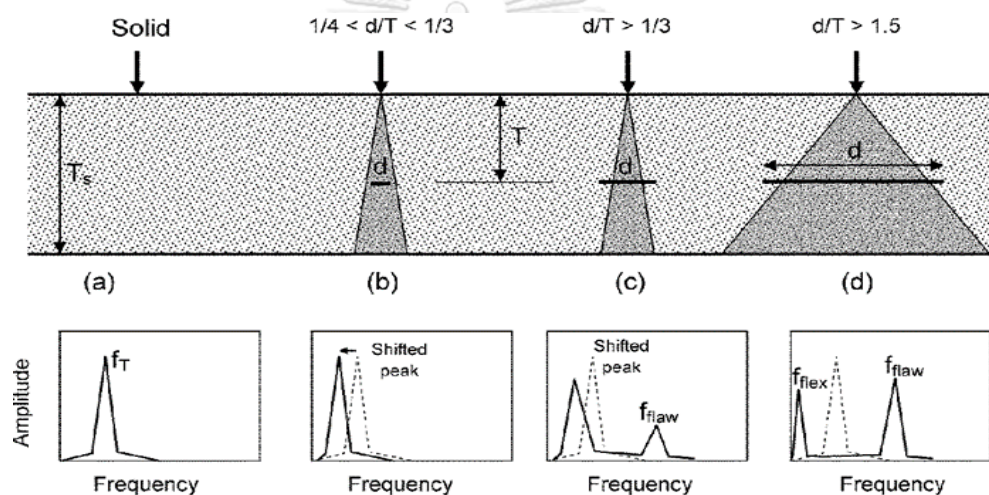


Figure 13. Schematic show different effects of relative flaw size on the impact-echo response (Carino, 2015).

The advantage of this method need not have a transmitting transducer due to generate pulse itself. Moreover, the stress pulse from this method has greater penetration ability and access only one side of the structural surface. Thus, it can widely use for detecting defects and structural thickness in plate-like structural members such as slabs and bridge decks. However, this method only generates at a point which does not focus like a pulse from an ultrasonic transducer, the pulse wave may arrive from many directions. Additionally, the limitation of this method is defect dimension ( $d$ ) which must greater than 0.25 of defect depth ( $T$ ), the defect can be detected as shown in Figure 13.

### 2.4.3 Ground penetrating radar (GPR) method

The GPR method is like the UPE method, but the electromagnetic (EM) waves are used instead of stress waves. The EM waves of the GPR method use radar frequency band,  $10^4$  to  $10^9$  Hz. At an early age, this method is specifically used for military applications especially bomb detection, and then continuously developed for evaluation of the concrete structure such as, concrete pavement thickness (Meyer et al., 2008), locating deteriorations and rebars (Lai et al., 2018), and locating utility networks (Jaw & Hashim, 2013; Metwaly, 2015). The GPR method and technique are widely used because of the ability to scan large areas while take a little time by emitting short pulses of EM waves and cost-effective.

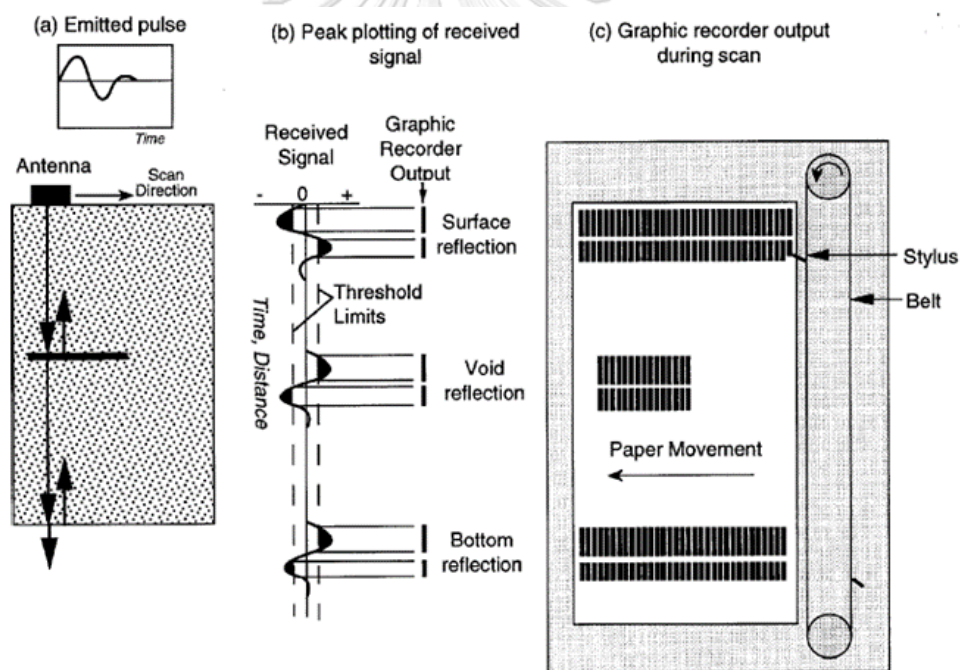


Figure 14. Three steps of the GPR method acquisition consist of a) schematic, b) received signal and graphic record output, and c) graphic recorder display a cross-sectional profile (ACI, 1998).

The testing principle of the GPR method is showed in Figure 14 which represents the wave propagation into the object by an antenna transmits short pulses of electromagnetic energy along the scan direction on the concrete surface. This

method need not prepare the concrete surface for testing because of no direct contact. The EM pulses travel through the material and then some wave energy reflected the antenna when encountering an interface between dissimilar materials. The material properties which affect the transmitted and reflected energy to the antenna are the dielectric constant and the conductivity. The definition of the dielectric constant is the amount of electrostatic energy stored per unit volume for a unit potential gradient and the conductivity is an electrical current capacity to flow through a material. After the reflection, the antenna generates an output signal proportional to the amplitude of the reflection. The output signal has information about wave velocity and attenuation. However, the quantities of the output signals depend on the electrical properties and the spatial configuration. The pulse duration of the concrete evaluation has often used the range from 1 to 3 nanoseconds and use nominal frequency values which appropriate types of geotechnical or structural survey (Venkateswarlu & Tewari, 2014) in the acquisition step. The electromagnetic wave speed (C) in a particular material is governed from the relative dielectric constants ( $\epsilon_r$ ) which is the ratio of material's dielectric constant ( $\epsilon$ ) to the free space's dielectric constant ( $\epsilon_0$ ) as shown in equation 7 to 8 and the example amount of relative dielectric constant of materials is shown in Table 3 below. Owing to the difference of relative dielectric constant of materials, the depth (D) of the reflecting interface is obtained from the two-way travel time (T) and the electromagnetic wave speed as shown in equation 9.

$$\epsilon_r = \frac{\epsilon}{\epsilon_0} \quad \dots\dots\dots (7)$$

$$C = \frac{C_0}{\sqrt{\epsilon_r}} \quad \dots\dots\dots (8)$$

$$D = \frac{CT}{2} \quad \dots\dots\dots (9)$$

Table 3. Relative dielectric constants and radar wave velocity are resulted from pulse-transmitted through the material.

Material	Relative dielectric constant of material, $\epsilon_r$	Radar velocity (m/ns)
Air	1	0.30
Water	81	0.03
Asphalt	2 to 4	0.15 to 0.21
Clay	2 to 10	0.05 to 0.21
Concrete	4 to 10	0.01 to 0.15
Granite	5 to 8	0.11 to 0.15
Limestone	4 to 8	0.10 to 0.15
Sand	4 to 6	0.12 to 0.15
Sandstone	2 to 3	0.17 to 0.21
Sandy soil	4 to 6	0.12 to 0.15
Clayed soil	4 to 6	0.12 to 0.15
Gravel	4 to 8	0.10 to 0.15

Furthermore, the amount of reflected energy, reflection coefficient ( $\rho$ ), determine from the ratio of the reflected the incident amplitude of the difference in the dielectric constant of material 1 ( $\epsilon_{r1}$ ) and 2 ( $\epsilon_{r2}$ ) as shown in equation 10 below. The difference in dielectric constant is previously identified what the material is by wave polarity. If the material 2 is greater than the material 1, the reflection coefficient is negative or strongly change the polarity at the interface such as the concrete-water interface and concrete-metal interface. This is the reason why the GPR method is very sensitive to metallic materials and moisture.

$$\rho = \frac{\sqrt{\epsilon_{r1}} - \sqrt{\epsilon_{r2}}}{\sqrt{\epsilon_{r1}} + \sqrt{\epsilon_{r2}}} \dots\dots\dots (10)$$

The components of measured devices composed of an antenna unit, a control unit, a display device, and a storage device refer to ASTM D4748 (ASTM, 2010). Firstly,

the antenna unit is the main part of emitting and receiving electromagnetic wave pulse due to the depth and resolution of this method are depending on the frequency content of the pulse (Venkateswarlu & Tewari, 2014). If it applies to the thin structural members or shallower detection, a higher frequency antenna is used for inspection. If it applies to the thick structural members or deeper detection, a lower frequency antenna is used for inspection. However, the actual penetration can shift or error detection due to the water content of the concrete (Kaplanvural et al., 2018). Secondly, the control unit controls the pulse by providing steady pulses, acquires the signal, and provides output to the display unit. The display unit shows the output signal by providing a cross-section that has a different color and pulse subtraction based on signal amplitude and polarity. Finally, the storage device keeps the signal data for later analysis and interpretation.

The advantage of this method need not contact antenna with the concrete surface thus it is very fast scanning and saving time. Moreover, it is very sensitive to detect metallic material and the presence moisture content. However, the output signal is a cone-shaped volume that can misinterpretation due to the dense of rebars or the performance from the service provider (Lai et al., 2018). Additionally, the deflection in the RC structure is not easy to detect because this method can penetrate across air layers.

## 2.5 Related Researches

Andrzej & Marta (2014) researched about structural integrity examination of concrete bridge structures by using the in-situ NDT methods. The research NDT methods used the IE method and the impulse response method for determining voids existed in tendon ducts on the road bridge localized near the Wizna village. The research conclusions reported that the combination method seems to be the most useful concept for structural integrity testing owing to they were confirmed accuracy and precision by the concrete core sampling method. However, NDT

methods have different advantages and limitations. If NDT methods were performed on larger areas to previously determine local areas with possible flaws, they recommended the impulse response method is more suitable than another one. However, they recommended the impact-echo method when detailed investigation of smaller areas were performed.

Azari et al. (2014) researched that the evaluation of concrete structures was carried out by the IE and UPV methods. The NDT methods were grid-testing performed on nine mock-up slabs with different thickness, and defects for creating contour maps. The contour maps of the IE and UPV methods exhibited in terms of dominant frequency and average modulus, respectively. The conclusion shows that the IE method provided the better results than the other while the simulated defects were deeper, but the reflected energy from the IE method was decreased while the thickness increased. Nevertheless, the combination methods were suggested to be more effective in locating the defects.

Clausen et al. (2012) researched onsite concrete quality assurance of concrete structure by using the IE and impulse response methods. The NDT methods were selected performed on columns, bridge decks, and pile for inspect injection quality, alkali-silica reactions and defects, and pile integrity, respectively. The research conclusions showed that the NDT methods provided clear results and quickly achieved the data. However, the NDT methods could be error localized when tested on an early stage of construction and time consuming when tested in large areas. The research recommended that data calibration should be done before acquiring the data.

Daungwilailuk et al. (2017) researched that evaluating damage concrete depth in the RC structures under different fire exposure time by using NDT and DT methods. This research focused on an assessment of fire-damaged RC slabs. The 10 RC slabs were constructed with two concrete grades of 24 and 35 MPa and the fire



test was selected test on only one side of the RC slabs under different times consist of 30, 60, 90, and 120 minutes. Then, the NDT methods compose of UPV and rebound hammer methods were performed. Besides, the DT methods compose of a pull-off test and core samples were performed to support and verify the results from the NDT methods. The research conclusion was reported that the compressive strength of 24 MPa specimens obtained higher results than 35 MPa specimens and the depth of the fire effect of 24 MPa is a lower degree of damage after fire testing. Additionally, the 30 minutes of heating time did not represent severe effects when compares with the other cases.

Hoegh et al. (2011) researched that the quality assurance and assessment of concrete pavement by ultrasonic tomography was generated by the UPE method. This research presented ultrasonic tomography through multiple field trials from both typical pavement constructability and rehabilitation by using MIRA equipment which generate low-frequency wave, 55 kHz, from 45 dry point contacts. In the past, the traditional ultrasonic method did not widely use in the concrete integrity of the pavement and some heterogeneous materials, due to other NDT methods such as the chain drags, and the IE method was enough. However, the new technique, ultrasonic tomography, data showed real-time and high resolution when were compared with the old previous methods via the ultrasonic profiles and were rechecked by concrete cores because of a multiple-static array of transducers. Besides, the conclusion exhibited that the ultrasonic tomography not only correctly determine reinforcement location and concrete pavement thickness but also located flaws such as delamination and degradation at the pavement joint.

Jaw & Hashim (2013) researched about accuracy located of underground utility by using GPR method due to urban expansion and development. This research used the IDS Detector Duo GPR equipment with two optimal frequency antennas, 250 MHz, and 700 MHz. This research previously studied the accuracy of three pre-

designed data acquisition scanning techniques compose of perpendicular to the pipe, along the pipe, and variation angles, and then the results of the previous part were applied to a real-world situation. The conclusion was demonstrated that both parts were shown good GPR mapping results while were scanned along with the pipeline scanning technique in the acquisition step.

Kaplanvural et al. (2018) researched about volumetric water content estimation of C-30 concrete by using the GPR method. This research acquisition used a 2.0 GHz antenna for estimating relative dielectric permittivity of the concrete block which knows water content by fitting the hyperbolas to the reflections. Moreover, data were acquired consecutively 5 times in each day within 150 days for estimating the water content of concrete change over time. The research conclusion were exhibited that the variation of relative dielectric permittivity is exponential decrease parallel with volumetric water content over time which is applicable for suitable setting up the GPR parameters at the other projects.

Lai et al. (2018) researched that the underground simulated voids under the concrete pavement were detected by the GPR method. The simulated air-filled voids were used plastic balls 0.62 m and 1.00 m diameter with different levels under the concrete pavement which has an approximate area 10.00x20.00 m. After that, they separated two teams with different criteria in data acquisition and interpretation steps and then the results were compared together by counting the score. The research conclusion reported that the voids or cavities under the concrete pavement could not be successfully detected by the GPR method from both teams based on five factor criteria which composed of the service provider (S), work procedure (W), instrument (I), materials (M), and specifications (S). However, the main factor effected to the quality of underground void detection was service provider.

Lorenzi et al. (2015) researched that determine the quality of concrete was carried out by the UPV method. This method was worldwide used because the abilities of this method could check variation in structures, presence of physical damages, measure thickness, and change of physical properties of materials. This research device used surface transducers with low-frequency range between 25 kHz to 60 kHz and was the grid-point measured range of 20x20 cm to 100x100 cm depending on the testing area for UPV mapping creation. Then, the UPV results from any points were generated to surface mapping represent the concrete velocity and improve the diagnostic by selected analyzing the concrete cores. The research conclusion reported that the UPV method had the capability to check the concrete condition because it was very sensitive to homogeneity and density variations.

Lybeart (2017) researched the analysis of concrete roads by the ultrasonic tomography method. This research object was compared the synthetic aperture focusing technique (SAFT) from two ultrasonic linear array devices which different from the transducer configuration composed of MIRA and PUNDIT PL-200 equipment. Both types of equipment were performed on six laboratory specimens which vary of thickness, reinforcement, and simulated defects and any field trails such as the motorway, and then the results were compared and rechecked with the pavement cores. The research conclusions displayed that both ultrasonic tomography devices can detect flaws with size greater than 40 mm, but the MIRA device can only detect the reinforcement and small defect with less than 25 mm. On the other way, many transducer configurations and higher frequency can be given higher detail and precision.

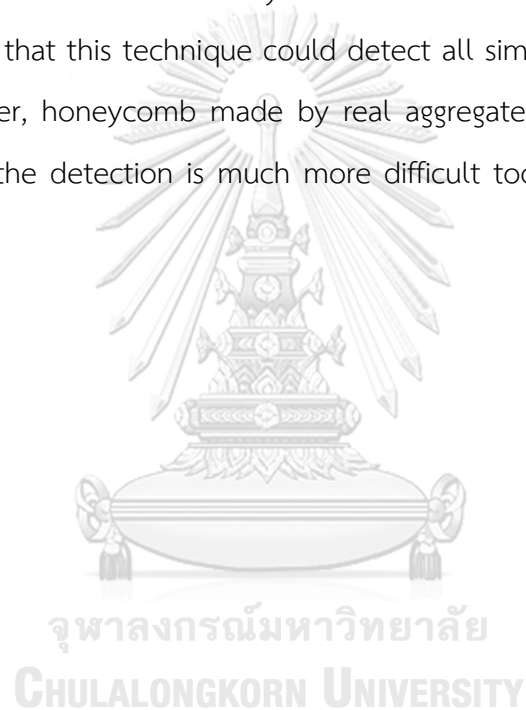
Metwaly (2015) researched that subsurface utility mapping by using the GPR technique before starting the excavation process. The research purpose was located the utility networks such as electricity cables, gas pipelines, fiber optic cables, water, and sanitary sewer pipelines, and street lighting circuits along the

second ring road in Holy Mecca city. The GPR method used a 400 MHz antenna for shallow subsurface investigation by transverse scan profiles along the asphaltic road. The research conclusions were demolished that the characteristics of hyperbolic reflected signals along any transverse profile scans can successively indicate the different subsurface utilities from the differences of sizes, shapes, and brightness of the reflected hyperbola.

Meyer et al. (2008) objected to accurately detect the thickness of concrete pavement sections by using the GPR method and then verified by a little of the core sampling method. This research used the SIR-3000 GPR equipment and a 1500 MHz antenna scanned all section pavements in 2 case studies. The first case study involved scans on a section of highway outside of Hooper, Nebraska to determine suitable dielectric constant values. The scan results showed weak signal reflections at the bottom of the concrete pavement, so the interpretation was difficult too. The second case study did like the previous case, but two metal rings were placed under the concrete pavement. The scan results showed a little high signal reflection around the metal rings which were a suitable material for providing an easier determination of the thickness.

Nguyen & Modrak (2018) reported that the comparison for defect detection in the concrete mock-up between two methods composed of Full-Waveform Inversion (FWI) and Reverse Time Migration (RTM) by using the UPV method. First, the FWI method was generated low-frequency wave, 40 kHz, at the concrete surface for preliminary concrete condition and large-scale defect detecting. Then, the RTM was generated high-frequency wave, 100 kHz, through the concrete too. However, it can detect only small-scale defects. Finally, all methods were tested on two types of concrete mock-up compose of inhomogeneous structure and layered structure. The results displayed that defect detection by the RTM method is greater than another method; however, the combined method gave the most accuracy and precision and save the testing budget too.

Stefan et al. (2018) reported about the validation measurement of artificial defects on reference structures by using the UPE method. The research equipment used transverse or shear waves with a very low frequency of 50 kHz for typical concrete investigation. This device was performed on the concrete mock-up with artificial defects such as delamination and honeycomb. The recommended materials for simulating the delamination and honeycomb were made by two concrete slabs attached to each other, and foam material and real aggregate, respectively, are intermediated layer between them. The research conclusion was displayed that this technique could detect all simulated defects in different levels. However, honeycomb made by real aggregate was closely like the real field defects, the detection is much more difficult too due to the scattering of elastic waves.



## CHAPTER 3 RESEARCH METHODOLOGY

The six steps of the research methodology are listed as follows 1) searching for theories and literature reviews, 2) searching for civil engineering data and any NDT equipment's procedures, 3) NDT test on RC mock-up simulated defects, 4) NDT test on RC structure which has defects, 5) interpretation and analysis the data, and 6) conclusion and presentation of the research. The details and flow chart of any steps will be described as follow.

### 3.1 Searching for Theories and Literature Reviews

The first key step is reviewing the related theories and literature in terms of theories, research objects, research methodologies, research results, research problems, and research limitations and recommendations as described in the previous chapter.

### 3.2 Searching for Civil Engineering Data and NDT Equipment

The second step of the research methodology searched the properties of good concrete which civil engineers must be considering, the factors that cause harmful defects to the RC structure or concrete deterioration, and the defects which often found in the RC structure.

In addition to this step was designed for the suitable methodology of any NDT types of equipment from the theories and literature reviews for data acquisition and interpretation steps. Then, they are practiced and found the limitations before acquisition with the idealized structures with simulated defects. The four NDT types of equipment that were selected in this research have the equipment details and procedures as the following description.

### 1) Ultrasonic pulse velocity (UPV) method

The PROCEQ's PUNDIT Lab equipment from Switzerland was used for the UPV method. This equipment composes of 2 transducers which be connected with display monitor by power cables. The transducers in this research use 54 kHz due to it can applicable with the most concrete application. The maximum grain size and minimum lateral dimension limitation of this transducer's frequency are approximately 34 mm and 69 mm, respectively.



Figure 15. PROCEQ's PUNDIT Lab and 54 kHz transducers are performed for UPV method ([www.proceq.com](http://www.proceq.com)).

The testing pattern was firstly set grid-point pattern on the testing surface every 0.10 to 0.20 m, and 0.50 m for the idealized structure and the realistic structure, respectively. Then, collecting time values from point-to-point testing with indirect transmission pattern as shown in Figure 6 in terms of time-domain and then transform it into pulse velocity. Finally, the velocity results at any point were plotted and classified concrete quality and were shown the results in the contour map.

## 2) Ultrasonic pulse-echo (UPE) method

The PROCEQ PUNDIT Live Array Pro from Switzerland was used for the UPE method. This equipment is multi-channel with 8 dry-point contact channels or a total of 24 dry-point contacts with frequency range is 15 to 100 kHz as shown in Figure 16 below. Thus, the cross-sectional profile result is a higher resolution when was compared to other types of equipment from different companies because the ray paths from all dry point contacts are 56 echoes in a matter of milliseconds. Moreover, the wavelength of this equipment is approximately 0.024 m to 0.160 m calculated from normally wavelength equation whereas shear velocity is 2,400 m/s. Thus, the minimum size of defects which this equipment can detect should be larger than wavelength and the ability for vertical and horizontal separation based on wavelength theory are 0.012 m and 0.006 m, respectively. Not only the results is a high resolution but also the acquisition step is suitable with all structures because it is not need both sizes of the structure for accessing. Last but not least, the maximum-depth detection of the equipment is 2.50 m which depending on the shear-wave velocity of the materials.



Figure 16. PROCEQ PUNDIT Live Array Pro wirelessly connect with tablet are performed for UPE method ([www.proceq.com](http://www.proceq.com)).



The testing pattern was firstly set line scans which were perpendicular together on the testing concrete surface every 0.10 m. and 0.50 m. for the idealized structure and the realistic structure, respectively. Secondly, the equipment wirelessly connects with the tablet before the acquisition of the data along with two-way direction line scans. Then, the data results along any line scans were shown in cross-sectional profiles represent reflection levels and intensities by changing color shading which relies on the difference of material properties. Finally, the reflection level of each point test along the line scans was created contour maps before comparison with other methods.

### 3) Impact echo (IE) method

The CTG-2 from Olson Instrument company, United States of America was used for the IE method. The equipment has a solenoid impactor to generate stress-wave by itself for concrete condition survey which thickness less than 1.80 m and an oscilloscope for expanding the signal before converting the data in terms of the time-domain to the frequency-domain by the Fast Fourier Transform. The frequency resolution of this equipment is 100 kHz. Another meaning is the wavelength of this equipment is approximately 0.036 m calculated from normally wavelength equation whereas compressional velocity is 3,600 m/s. Thus, the minimum size of defects which this equipment can detect should be larger than wavelength.



Figure 17. Impact Echo connect with tablet are performed for IE method ([www.olsoninstruments.com](http://www.olsoninstruments.com)).

The testing pattern was firstly set grid-point pattern on the testing concrete surface like the ultrasonic pulse velocity method. Secondly, the equipment related to the tablet by the power cable before the acquisition. Then, the results at any point were displayed in 2 typical graphs compose of 1) voltage vs. time graph and 2) amplitude vs. frequency graph. However, the interpretation of waveforms in the time domain is feasible, the interpretation by frequency analysis is a preferable approach. Thus, the concrete condition at any point can be classified from changing and shifting of the frequency amplitude. Finally, the highest peak of the frequency of each point test was created contour map before comparison with other methods.

#### **4) Ground penetrating radar (GPR) method**

The PROCEQ GPR Live from Switzerland was used due to the unique stepped-frequency continuous-wave (SFCW) technology as shown in Figure 18. The inside of the equipment has multiple separate antennas in the range of 0.20 to 4.00 GHz which can widely detect different materials, but the central frequency value is 2.40 GHz or 2400 MHz which suitable with a structural survey. The advantages of ultra-wideband technology are higher penetration depth and resolution results as shown in Figure 19. Moreover, the wavelength of this equipment is approximately 0.0045 m calculated from normally wavelength equation whereas velocity is 0.11 m/ns. Thus, the minimum size of defects which this equipment can detect should be larger than 0.0045 m and the ability for vertical and horizontal separation based on wavelength theory are 0.00225 m and 0.001125 m, respectively. However, the maximum-depth detection of the equipment is 0.70 m depending on the dielectric properties of materials.



Figure 18. PROCEQ GPR Live wireless connect with tablet for GPR method (www.proceq.com).

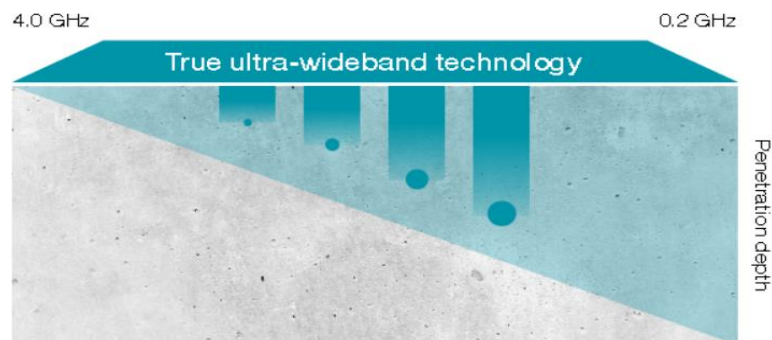


Figure 19. the cross sectional profile illustrate the resolution depth due to the ultra-wideband technology (www.proceq.com).

The testing pattern was firstly set line-scan pattern on the testing concrete surface at every 0.10 m. Secondly, the equipment was wirelessly connected with the tablet before the acquisition of the data by transmits EM pulses along the two-way direction lines. Then, the results along any line scans were shown in a cross-sectional profile that represents reflection levels and intensity which rely on the difference of the dielectric constant and conductivity of the materials. Finally, the application automatically generates an area scan by a combination of all the perpendicular line scans before were compared with other methods.

### 3.3 NDT on RC Mock-Up Simulated Defects Step

Reinforced concrete slabs on beams were firstly designed and then were constructed to simulated various sizes, dimensions, and shapes of artificial defects. The specimen configurations were nominally designed to 0.30 m thick with lateral dimensions of 0.80x1.20 m supported with two parallel beams which have dimensions of 0.15x0.50 m. Ready-mixed concrete was designed used 280 ksc or 27.5 MPa. The concrete was made with limestone aggregate as normally used in Thailand. Moreover, the RC slabs are reinforced in two dimensions with spacing every 0.20 m and at two layers by deformed bar size 12 mm. The designated concrete covering of the upper and lower-layer rebar was 4.00 and 5.00 mm, respectively as shown in the plan and two-section views in Figure 20.

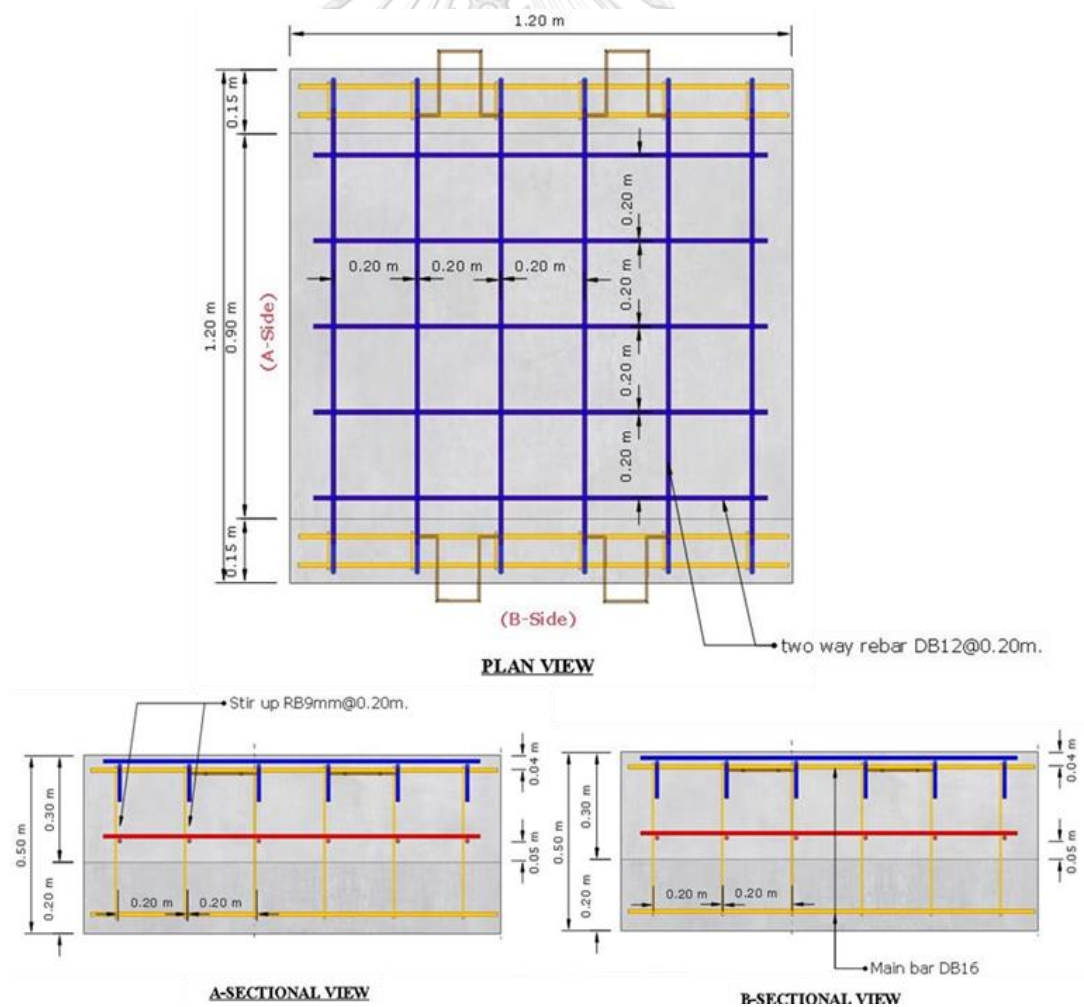


Figure 20. The designation of RC mock-up shows on plan and sectional views.

After the construction of idealized structures was already finished, they were set the testing patterns which have both grid point and line scan. Then, the signal data was acquired by all NDT equipment as previously described at 7, 14, 28, and 56 concrete day-life.

### 3.4 NDT on RC Structure Step

The realistic structures were previously selected by gathering information and background documents and then did preliminary works compose of visual inspection and hammer sounding. The research RC structures could have defects that were observed with the naked eye refer from ACI 201.1R as shown in Figure 21 and supported with ringing sound by hammer hit on the concrete surface refer from ASTM D4580 for scoping testing areas. Then, all equipments based on NDT method were performed as same as an RC mock-up step.

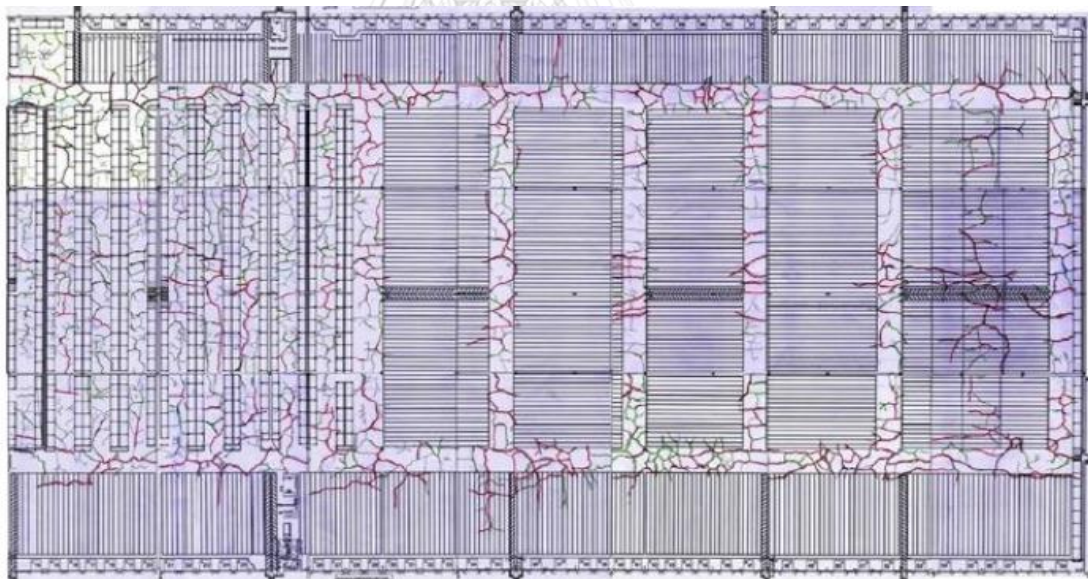


Figure 21. The example plan of realistic structure was illustrated crack lines on slab (Zoidis et al., 2013).

### 3.5 Interpretation, Analysis, and Discussion Step

These have two parts for analysis and interpretation of the NDT signals from both the idealized structures and the realistic structure which have details as the following description.

First of all, the acquisition data of any equipment based on NDT method from the four RC mock-ups were analyzed and interpreted over the difference of concrete day life, hardening period. The using parameters which were calibrated with known concrete thickness were changed over the hardening period due to the changes of material components and properties especially water content in the concrete. Thus, the RC mockup results were previous guidelines for setting suitable parameters which were related with types of structure and concrete day-life, and testing patterns which were related with structural depth and dimension. Moreover, Example of NDT signals when flaws were detected can be guidance for the realistic structure too.

Then, the acquisition data of any equipment based on NDT method from the realistic structure which have defects or damages were analyzed and interpreted for locating flaw positions and scoping flaw areas by using signal guidelines, pulse criteria, and suitable parameters were set refer from the idealized structures. The NDT signals or results from this step were compared with the idealized structure when they were maybe detected the flaws in concrete. In addition, concrete core positions were randomly selected by differences of NDT results to verify correctness.

In conclude, all the results from two parts were combined and compared to any NDT methods that were discussed in terms of accuracy, precision, duration, limitation, management, and interpretation.

### 3.6 Conclusion and Presentation Step

The descriptive comparison results were finally concluded and discussed what NDT method in this research is the best for inspection and evaluation of air-filled void and delamination in concrete. In addition, the research limitations and obstructions were concluded and recommended for further studies. Last but not least, this research was published in the academic journal and presented in the academic conference.

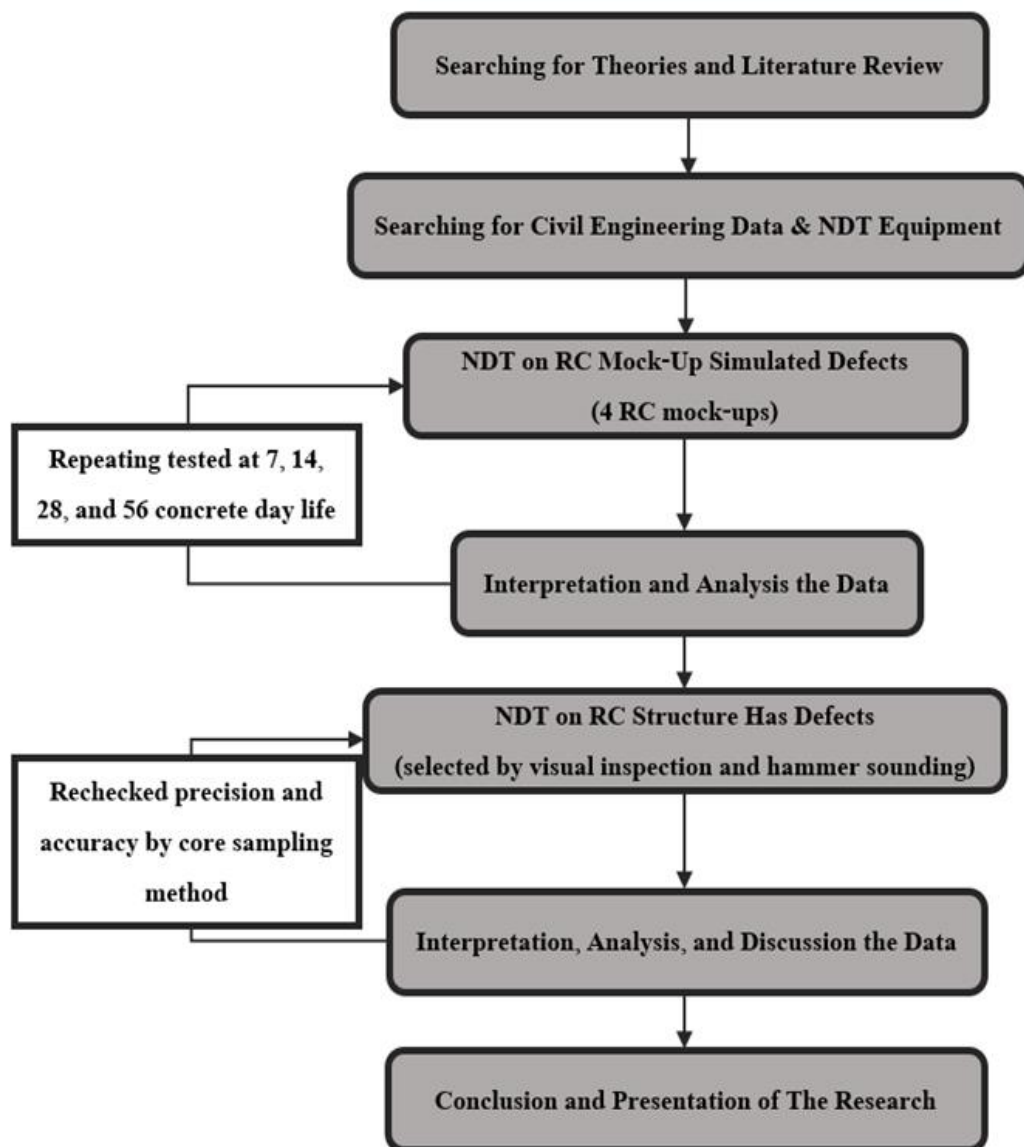


Figure 22. Flow chart exhibit 6 steps of research methodology.

## CHAPTER 4 RESEARCH RESULTS

### 4.1 Details of RC Mock-Up Simulated Defects

Totally four RC concrete slabs on the beam were constructed to simulated various sizes, dimensions, and shape of artificial defects which composed of 1) delamination, 2) air-filled void, 3) delamination and air-filled void, and 4) unconsolidated concrete as shown in Figure 23. The simulated defects in this research were constructed from three different types of materials. First of all, delamination was imitated by using 3.00 mm and 6.00 mm square plastic boards at the rebar level on both sides of the RC mock-up. Then, air-filled voids were constructed by using 5.00 to 15.00 mm low and high-density foam blocks spread in the RC mock-up. Lastly, unconsolidated concretes or honeycombs were constructed by pouring concrete on sieving shuttering. Table 4 was provided a summary of the RC mock-up details and Figure 24 was shown the simulated defect position on the plan view. Thus, the testing area on each mock-up was approximately sized of 0.80x1.00 m (Width x Length) which were excluded supported RC beams and 0.10 m from the edge of structures.



Figure 23. Totally four RC mock-ups with simulated defects were constructed.



Table 4. Simulated defect positions were concluded from four RC mock-up.

Mock-up name	Defect number	Material thickness (mm)	Defect type	Defect dimension (mm)	Defect depth (mm)
Delamination	No. 01	6.00 mm. Plastic board	Delamination	200x200	40.00
	No. 02	6.00 mm. Plastic board	Delamination	200x200	30.00
	No. 03	3.00 mm. Plastic board	Delamination	200x200	40.00
	No. 04	3.00 mm. Plastic board	Delamination	200x200	30.00
	No. 05	3.00 mm. Plastic board	Delamination	200x200	220.00
	No. 06	6.00 mm. Plastic board	Delamination	200x200	250.00
	No. 07	3.00 mm. Plastic board	Delamination	200x200	220.00
	No. 08	3.00 mm. Plastic board	Delamination	200x200	250.00
	No. 09	3.00 mm. Plastic board	Delamination	200x200	220.00
Air-filled void	No. 01	15.00 mm high dense foam	Air-filled void	200x200	110.00
	No. 02	5.00 mm high dense foam	Air-filled void	200x200	90.00
	No. 03	10.00 mm low dense foam	Air-filled void	150x150	150.00
	No. 04	10.00 mm low dense foam	Air-filled void	150x400	200.00
	No. 05	5.00 mm high dense foam	Air-filled void	200x200	70.00
	No. 06	15.00 mm low dense foam	Air-filled void	200x300	100.00
Delamination & air-filled void	No. 01	3.00 mm. Plastic board	Delamination	200x400	60.00
	No. 02	3.00 mm. Plastic board	Delamination	200x400	40.00
	No. 03	10.00 mm low dense foam	Air-filled void	400x600	120.00 to 180.00
	No. 04	3.00 mm. Plastic board	Delamination	200x400	270.00
	No. 05	3.00 mm. Plastic board	Delamination	200x400	250.00
Unconsolidated concrete	No. 01	50.00 mm. concrete	Honeycomb	200x200	190.00
	No. 02	50.00 mm. concrete	Honeycomb	200x200	190.00
	No. 03	50.00 mm. concrete	Honeycomb	200x200	190.00
	No. 04	50.00 mm. concrete	Honeycomb	200x200	190.00

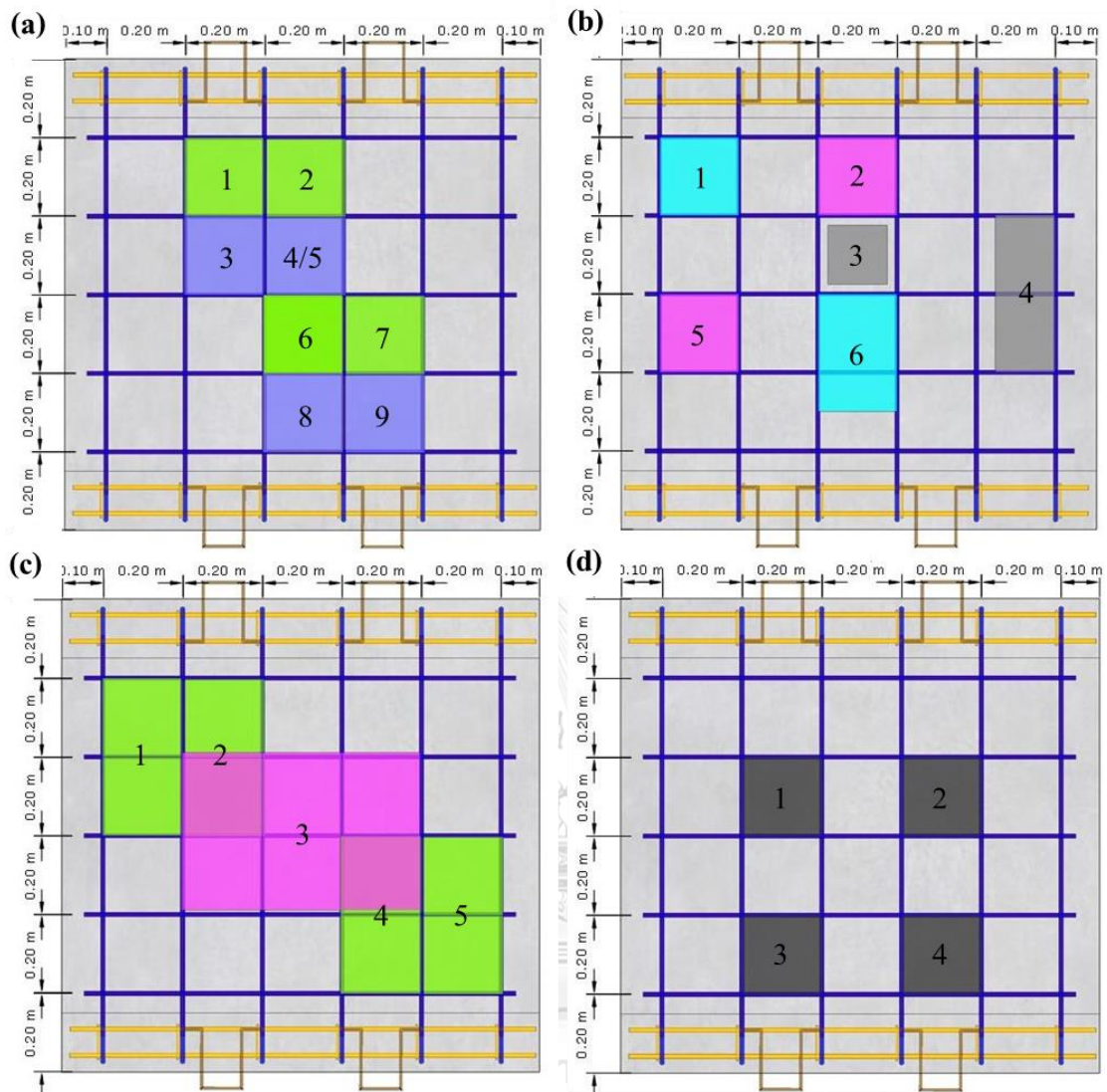


Figure 24. Plan views illustrate number of simulated defects from any mock ups composed of a) delamination, b) air-filled void, c) delamination and air-filled void, and d) unconsolidated concrete.

The unconsolidated concretes as shown in Figure 25 were showed the differences of void and concrete ratio from poor concrete quality to moderate concrete quality which were only classified by eyesight owing to this research was not contained the measurement of the void and concrete ratio.



Figure 25. Four unconsolidated concretes illustrate the difference of void and concrete ratio by naked eyes.

#### 4.2 Results of NDT Signals on RC Mock-Ups

After the idealized structures were already constructed, the NDT types of equipment that were previously described in chapter 3 were performed on all the RC-mock ups simulated defects in the different concrete day-life at every 7, 14, 28, and 56 days. All NDT types of equipment must be previously calibrated with known concrete thickness for setting suitable parameters in each the hardening period before data acquisition. Due to, the results in this part have too much data over the hardening period, they were selected displayed in this research. The results were orderly shown from line-scan testing pattern to grid-point testing pattern, respectively.

##### 1) Line-scan testing pattern

These line-scan results were displayed the selected cross-sectional profiles from both GPR and UPE methods over the hardening period. The line-scan results in this section were performed perpendicular together which have spacing about 0.10 m. However, the acquiring sensors inside of both methods and dimensions of the equipment are not similar, the differences of line-scan testing patterns were compared and shown in Figures 26 and 27 between both methods.

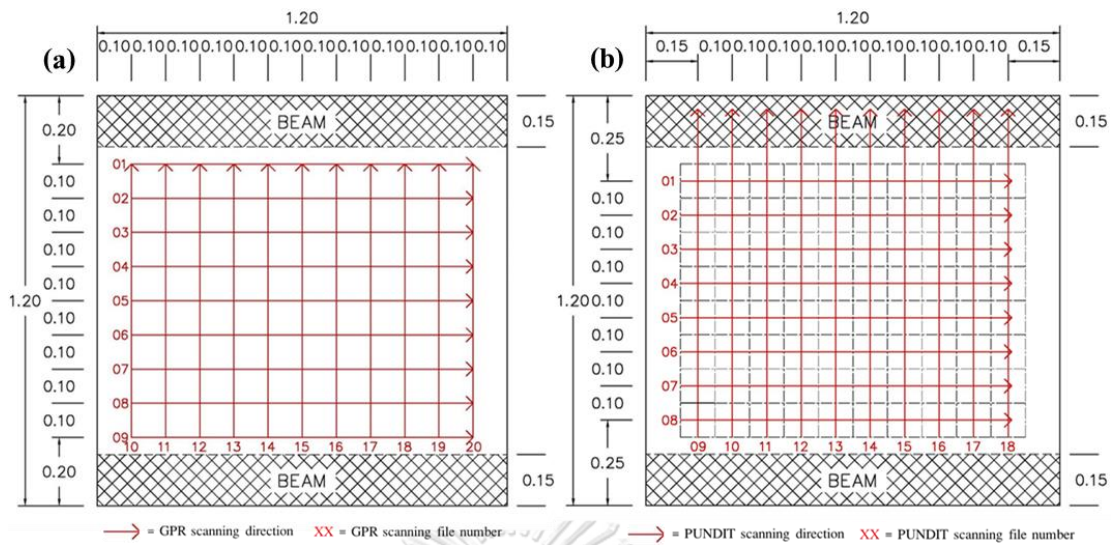


Figure 26. Plan views illustrate line-scan testing patterns of a) GPR and b) UPE methods.

Then, the suitable parameters of the GPR and UPE methods were calibrated with known concrete thickness over the hardening period. The dielectric constant parameter of the GPR method was shown that it was significantly decreased which were changed values from 8.8, 8.3, 8.2, and 7.5 over the hardening period due to the evaporation process or loss of water-concrete ratio. Thus, all GPR profiles were displayed better resolution as clearly display the thickness level along cross-sectional profiles when the concrete is getting older. The shear-wave speed values of the UPE method are approximately used valued at 2,360, 2,410, 2,486, and 2,453 m/s over the hardening period. The UPE parameter shows that it quietly constant over time. Moreover, the UPE cross-sectional profiles have been still displayed good resolution since the recently hardening period, at 7 concrete day life. Figure 28 to 31 are shown the comparison on selected cross-sectional profiles of each mock-ups between the GPR and UPE methods over the hardening period.



Figure 27. Line-scan testing over the hardening period was performed by GPR and UPE methods.

The comparison between both methods on mockup no.01 over the hardening period clearly showed that the simulated delamination can be detected. The quality of GPR profiles along line scan no.15 was higher resolution over the hardening period; nevertheless, the shallow defects were only clearly detected. The weak of the propagated wave, the level and dimension of defects were maybe the reasons why the deep level of defect cannot clearly detect like the shallow one along the GPR profile. However, the deep delamination can be only detected at 58 concrete day-life. The other meaning is the GPR method can successfully detect the deep defects in realistic structure too. On the other hand, the UPE profiles along the line scan no.14, close up with the GPR line scan, have been clearly showed all the defect levels and positions since the 7 days. However, they have only displayed the reflection level at deep defects. The level of shallow defects was not clearly showed along the cross-sectional profile but another criterion which could be indicated to represent them is the disappearance of the reflection level at the concrete thickness. In conclusion, the flaw detection of mock-up no.01 is shown that both methods are

successful detection along the hardening period but the GRR resolution is the most highest when the concrete day-life is older than the hardening period.

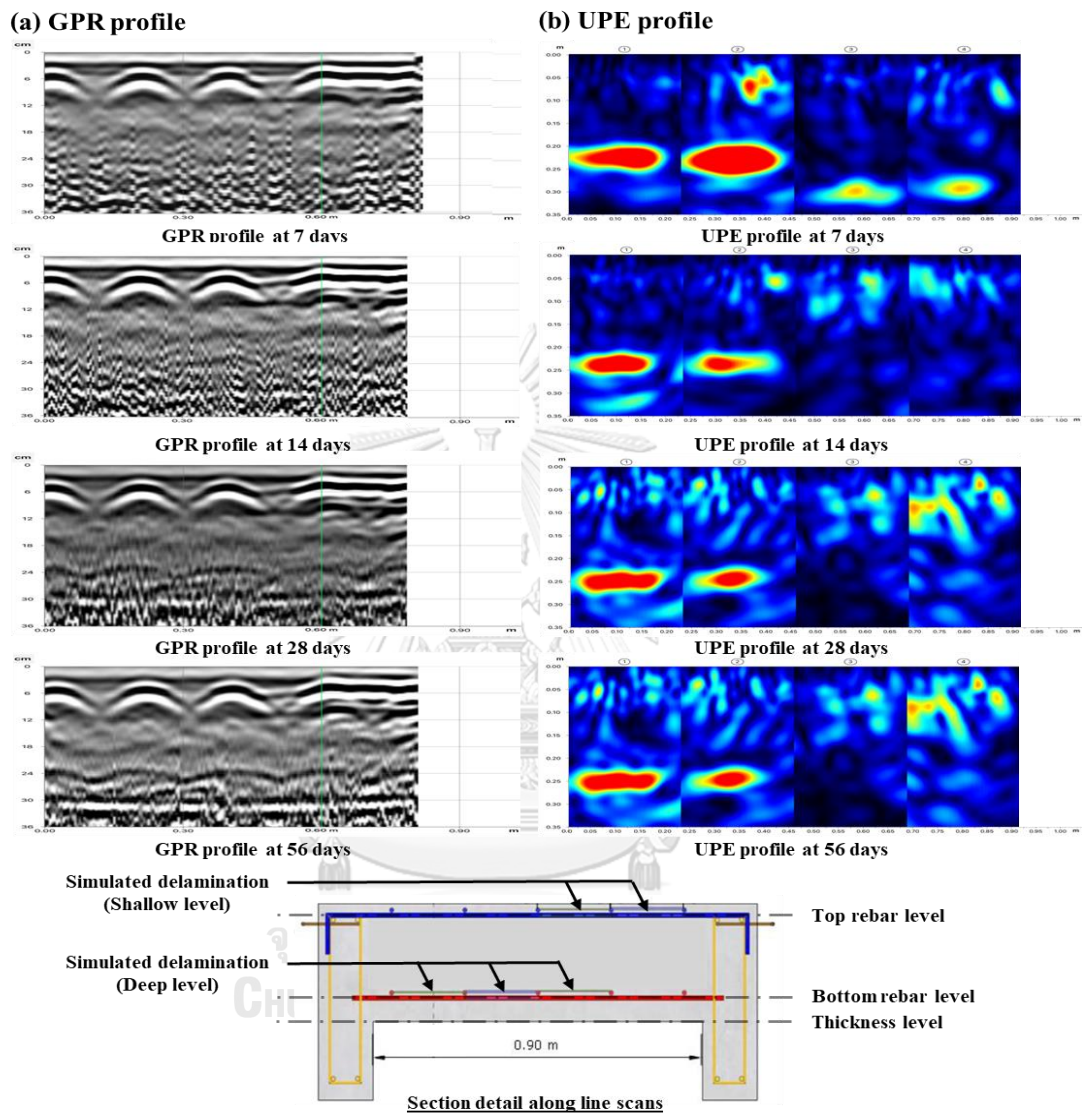


Figure 28. Selected a) GPR and b) UPE cross-sectional profiles on mock-up no.01 were compared results over hardening period with cross-section detail.

The comparison between GPR and UPE methods which were resulted from line scan no.15 and no.14, respectively on mock-up no.02 over the hardening period is clearly showed the level of simulated defects. However, the small defect at the lower level, at the middle between both upper levels, cannot be detected from both methods. It may be theoretically caused by small, simulated defects which less

that Fresnel zone or a quarter of wave, and wave diffraction at the edge from the upper level of simulated defects or it was out of the position which was resulted from construction. In addition, the signal characteristic of the UPE method was changed which were showed multiple reflections due to the simulated defects were thicker than the mock-up no.01. In conclusion, the flaw detection of mock-up no.02 is shown that both methods are successful detection along the hardening period.

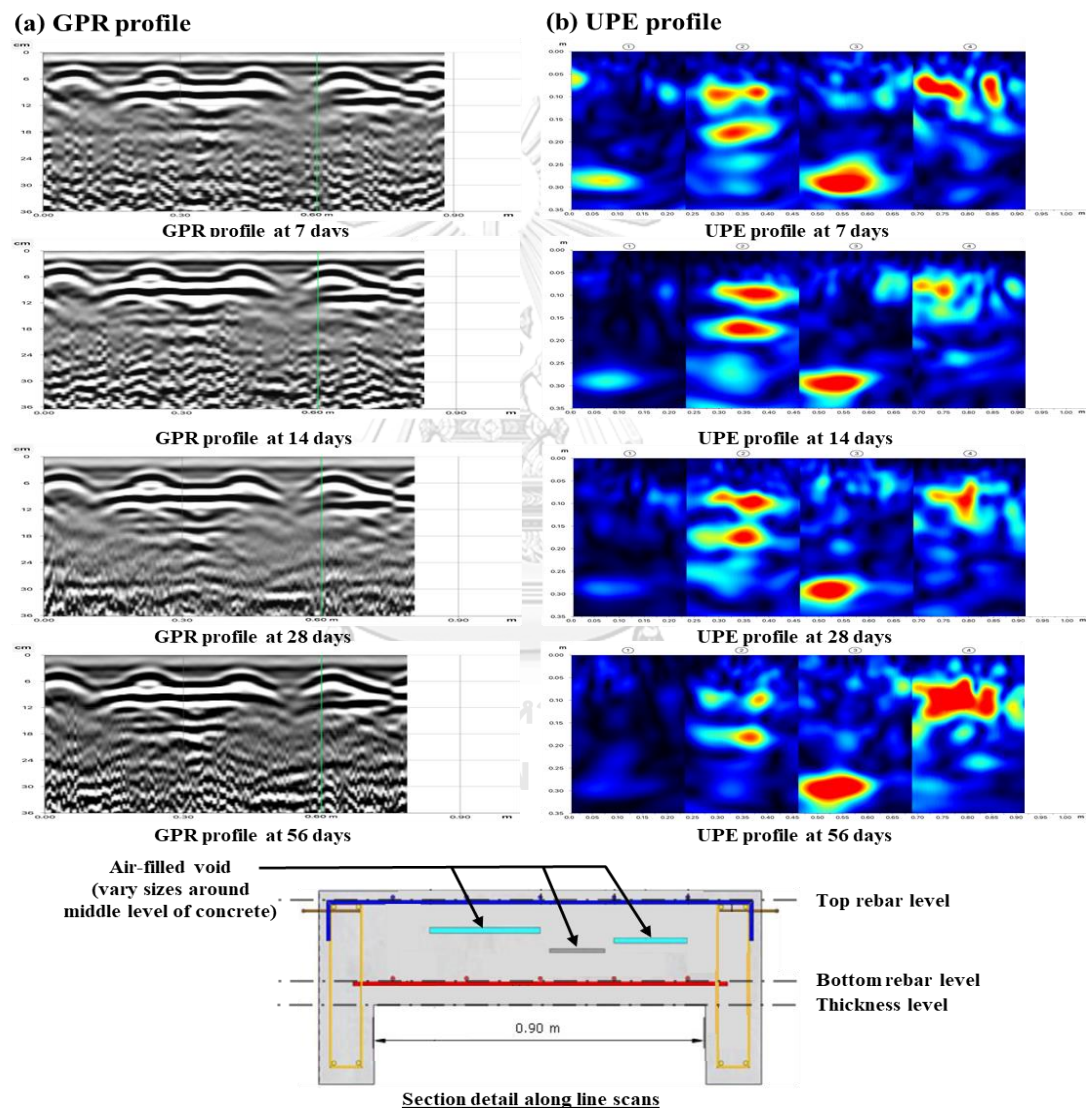


Figure 29. Selected a) GPR and b) UPE cross-sectional profiles on mock-up no.02 were compared results over hardening period with cross-section detail.

The comparison between GPR and UPE methods which were resulted from line scan no.6 and no.5, respectively on mock-up no.03 over the hardening period clearly displayed the middle level and curved shape of the simulated air-filled void. The lowest level of defects cannot be detected from the GPR methods; however, they can be detected by the another. Moreover, the deep defect that was laid below the simulated air-filled void cannot be detected by both methods. The brightness reflection signal at shallow level on the left side of the UPE profile is the positions of shallow simulated delamination which are not shown on the GPR profile due to the shifted line scan. In conclusion, the flaw detection of mock-up no.03 is shown that both methods are successful detection along the hardening period.

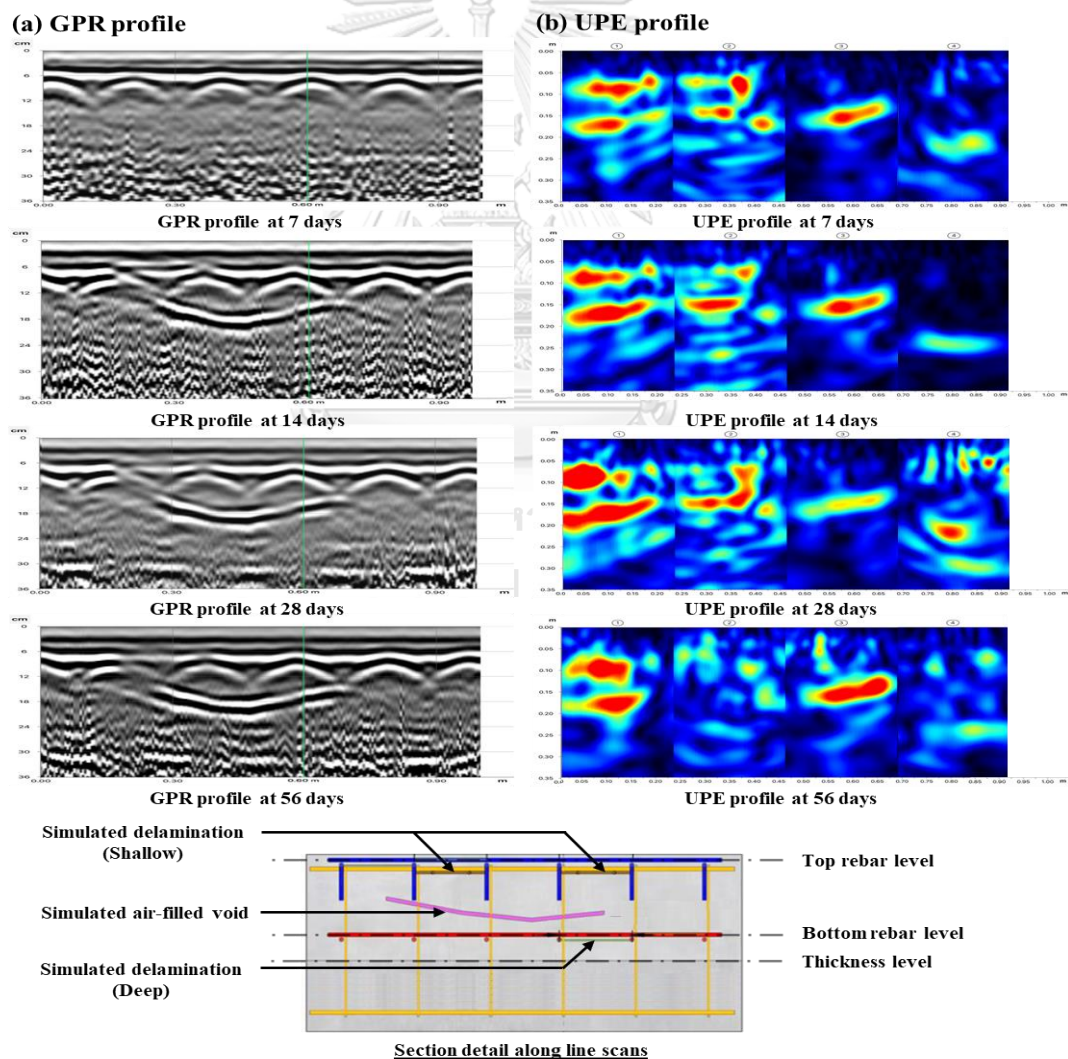


Figure 30. Selected a) GPR and b) UPE cross-sectional profiles on mock-up no.03 were compared results over hardening period with cross-section detail.



The comparison between GPR and UPE methods which were resulted from the similar line scan no.7 on mock-up no.04 over the hardening period cannot display the level of defects. Simulated unconsolidated concretes which were laid on the lower rebars cannot be detected by both methods maybe cause of the limitation of the equipment's detection and/or too small size of air-bubble in the simulated samples. In conclusion, the flaw detection of mock-up no.03 is shown that both methods are not successful detection along the hardening period.

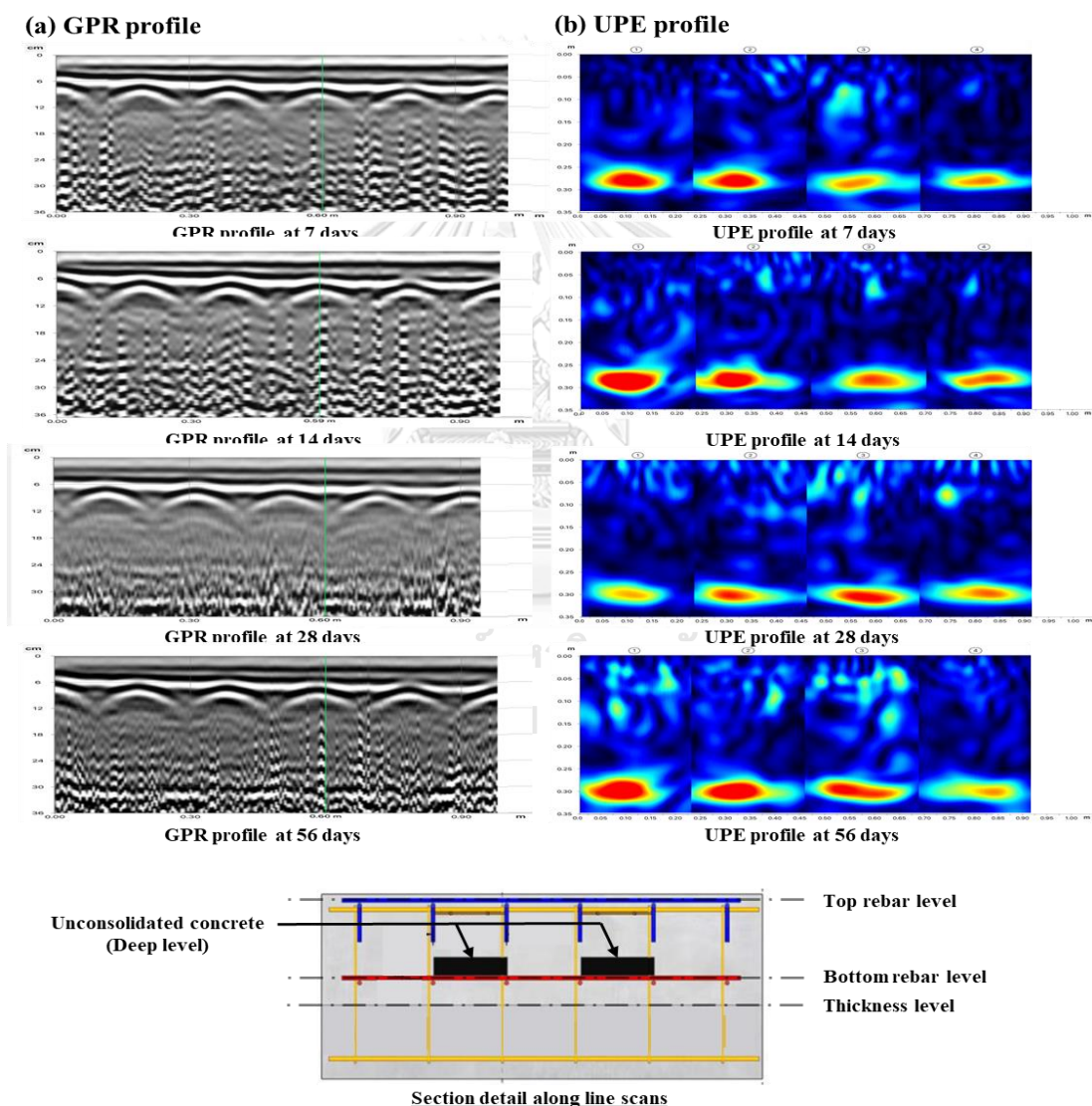


Figure 31. Selected a) GPR and b) UPE cross-sectional profiles on mock-up no.04 were compared results over hardening period with cross-section detail.

Although the cross-sectional profiles were clearly shown the levels and positions of simulated defects by signal brightness refer from reflection coefficient equation when the wave faces dissimilar layers. Nevertheless, they would like to be created contour maps for comparing the results with other NDT methods in this research.

## 2) Grid point-testing pattern

The grid point-testing results were displayed the example data from IE and UPV methods over the hardening period. The grid-point results in this section were performed at every point which has spacing between 0.10 to 0.20 m. However, both methods have the differences in acquisition steps which were compared and shown in Figures 32 and 33 between both methods.

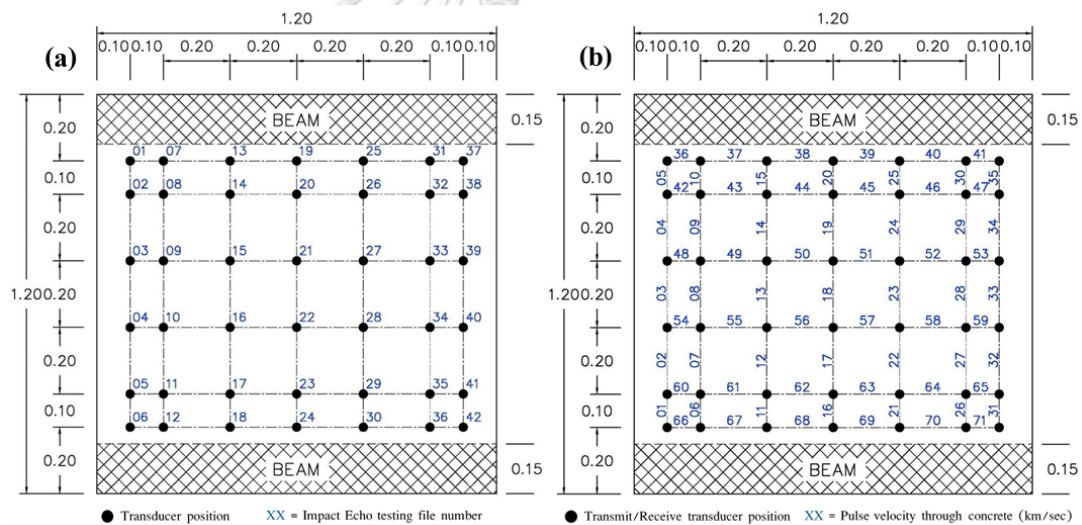


Figure 32. Plan views illustrate point testing patterns of a) IE and b) UPV methods.

After that, Only the IE method must be calibrated with known concrete thickness for finding suitable the compressional-wave velocity. The values are setting at 3,476, 3,604, 3,604, and 3,656 m/s over the hardening period from younger to older concrete, thus the thickness frequency values should be in the range of 5.8 to 6.3 kHz as shown in Figure 34. It was quite as same as the UPE method; however, the velocity values were greater because of the relationship between P-wave and S-

wave. Owing to the wave speed and thickness frequency from testing are known, the reflection depth was calculated based on equation 6. If the thickness and dimension of simulated defects is larger enough which the equipment could detect, the thickness frequency was shifted to be a higher frequency value or reflection level is shallower than the previous describe as shown in Figure 35. However, any frequency profiles were shown the peak amplitude out of the thickness range, this type of signal means the shallow defects or delamination are found less than approximately 100.00 cm. which call “Flexural frequency mode” as shown in Figure 36.



Figure 33. Line-scan testing over the hardening period was performed by IE and UPV methods.

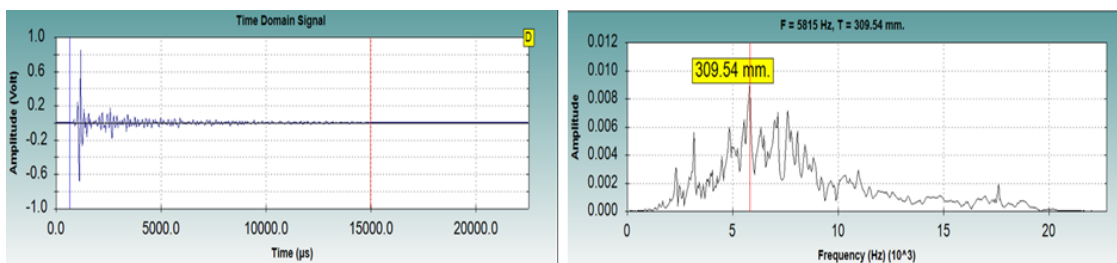


Figure 34. Exemplar result of thickness frequency was inspected by IE method.

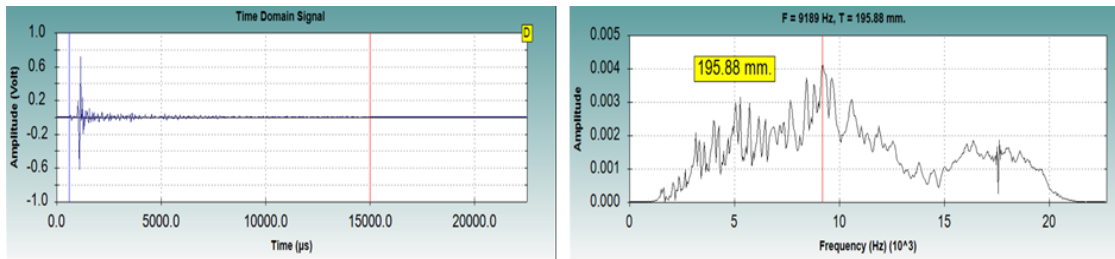


Figure 35. Example result of shifted frequency was inspected by IE method.

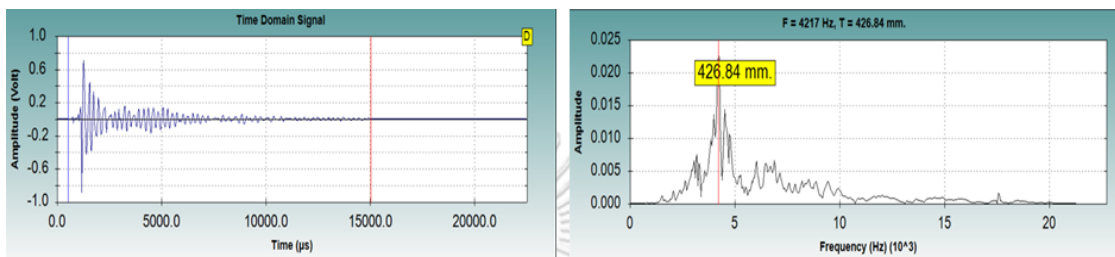


Figure 36. Example result of flexural frequency was inspected by IE method.

The UPV method was calibrated itself so it need not to know the concrete thickness. It only focuses on the travel time between transducers at any point with known the path ranges for calculating wave velocity. Thus, the concrete quality at any point can be classified as referring from Table 2. Nevertheless, the UPV results cannot be located the deflection level and cannot deeply penetrate the signal through the concrete because the indirect configuration, the same side of transducers, was performed. In conclusion, the UPV results can be only shown wave velocity transmitted between the transducer probes by contour map of concrete integrity level.

Although the results from almost equipments based NDT methods in this research were successfully detected flaw or defect positions, they cannot be interpreted and analyzed the results all together. Thus, the proper methods for interpretation over the hardening period would like to be generated contour maps which were represents the reflection level. Thus, Figure 37 to 40 are illustrated the contour maps over the hardening period of each RC mock-ups simulated defects from no.01 to no.04, respectively, which have different things as be described below.

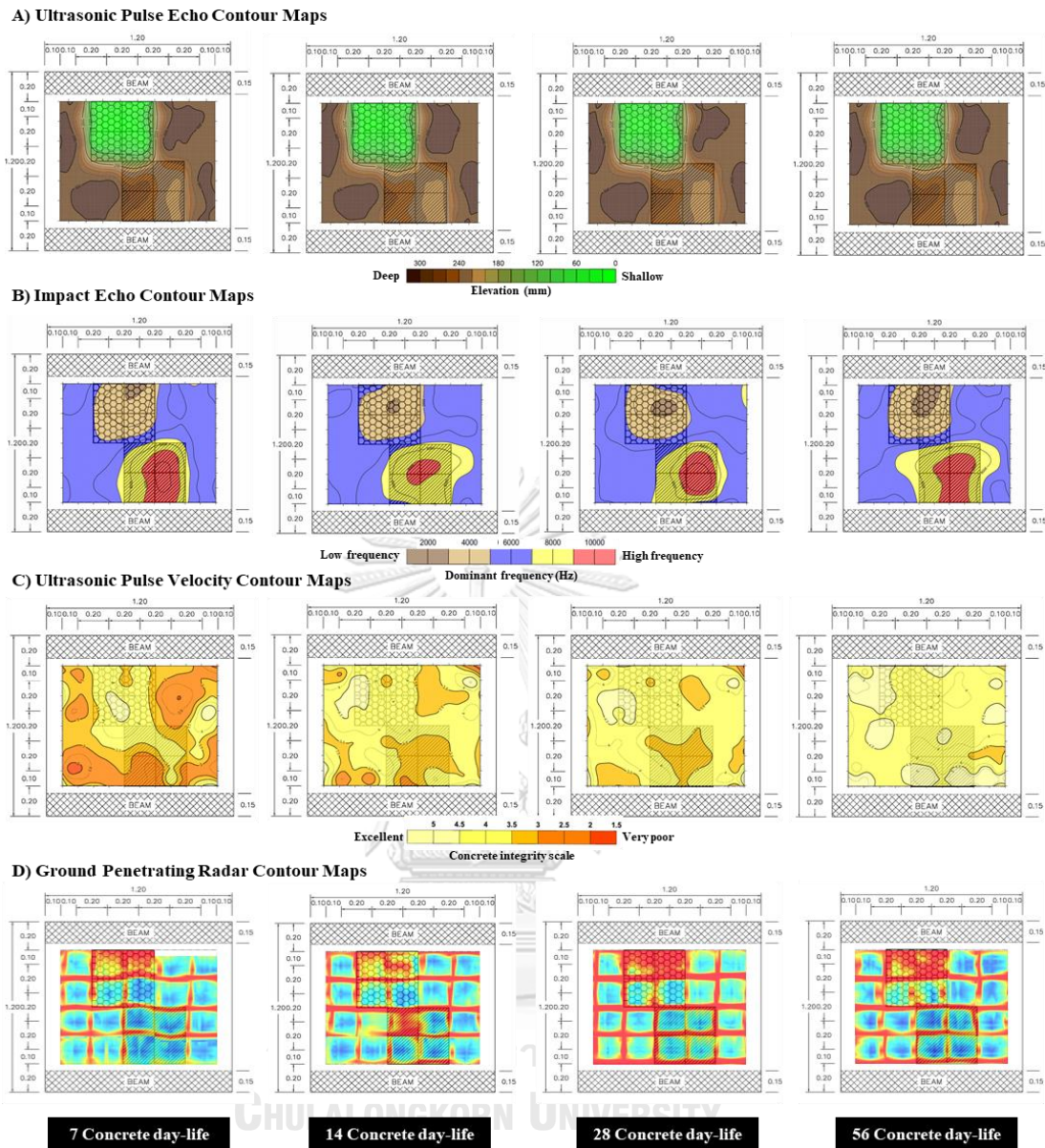


Figure 37. All NDT contour maps of mock-up no.01 were illustrated over hardening period.

First of all, the comparison of grid-point testing methods from mock-up no.01 was shown that the IE method is more successfully detected and scoped at all levels of the simulated delamination than the UPV method. However, UPE contour maps show all reflection level of them as same as the IE method, the UPE precision and accuracy of flaw detection is better. Then, GPR contour maps are not successful method because they only represent some parts of the upper-simulated

delamination over the hardening period. Nevertheless, the GPR profile as previous describe show the weakly deep reflection, so the interpretation of the GPR method be rechecked with the cross-sectional profile for better precision and accuracy. In conclusion, the ability of defect detection of any NDT methods on the mock-up no.01 can be orderly accuracy, precision, and performance by UPE = IE > GPR > UPV methods along the hardening period.

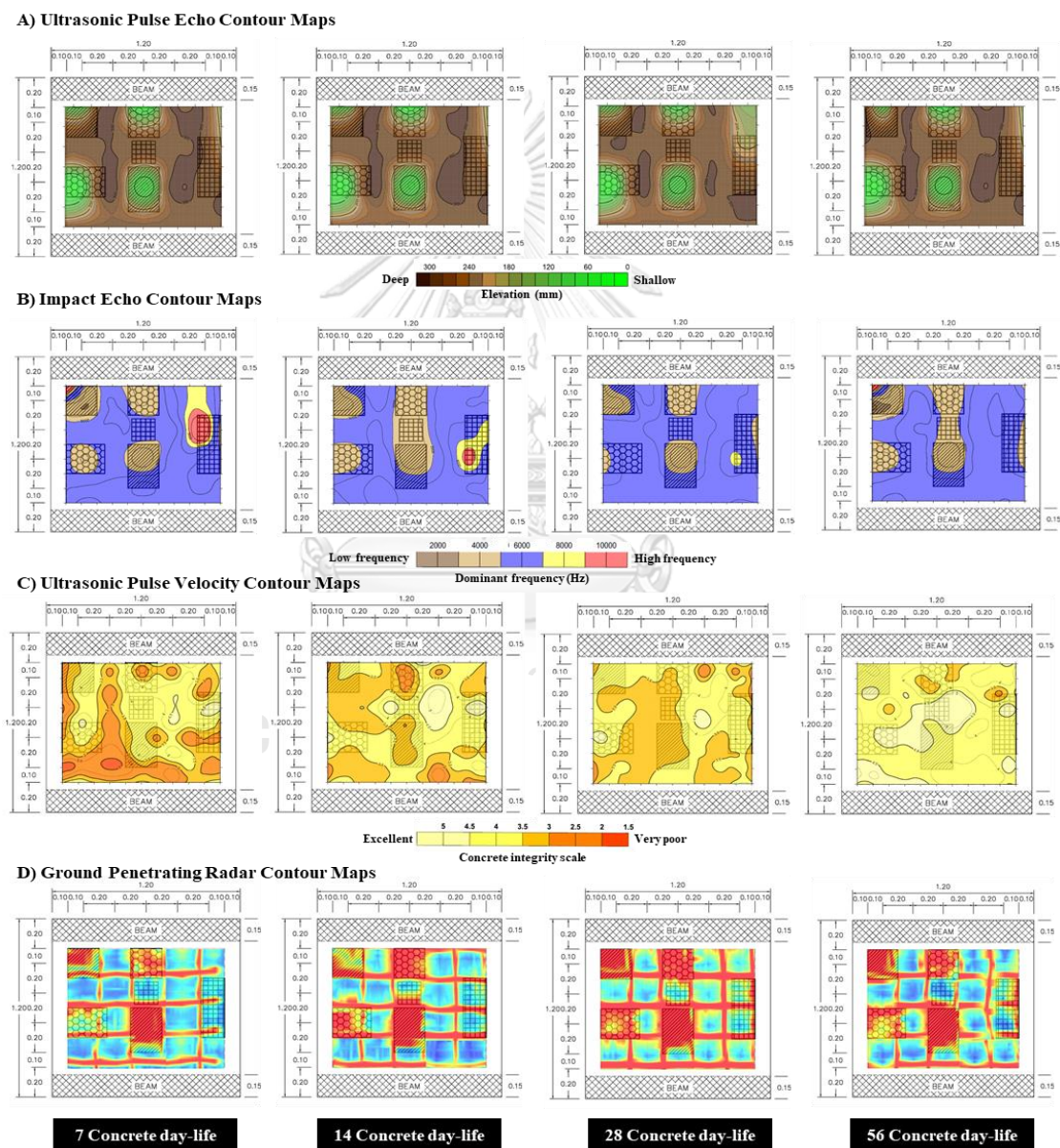


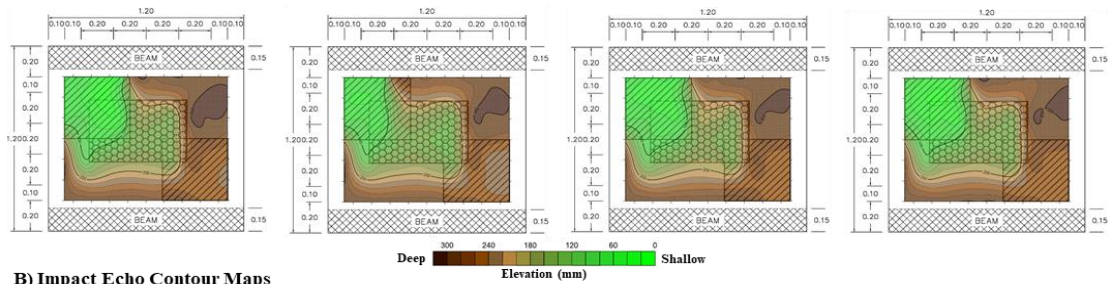
Figure 38. All NDT contour maps of mock-up no.02 were illustrated over hardening period.

Secondly, the comparison of grid-point testing methods from mock-up no.02 show that the IE method is more successfully detected in the simulated air-filled voids than the UPV method again. However, the IE contour map cannot show the deep simulated defects as similar as the UPE contour map. Moreover, the GPR contour map show almost simulated air-filled voids over the hardening period except the deepest one as same as UPE and IE methods. Almost equipments based NDT method could not detect the deepest air-filled void which was maybe laid on the lower level of rebars around the edge of the testing area. In conclusion, the ability of defect detection of any NDT methods on the mock-up no.02 can be orderly accuracy, precision, and performance by  $UPE = GPR > IE > UPV$  methods along the hardening period.

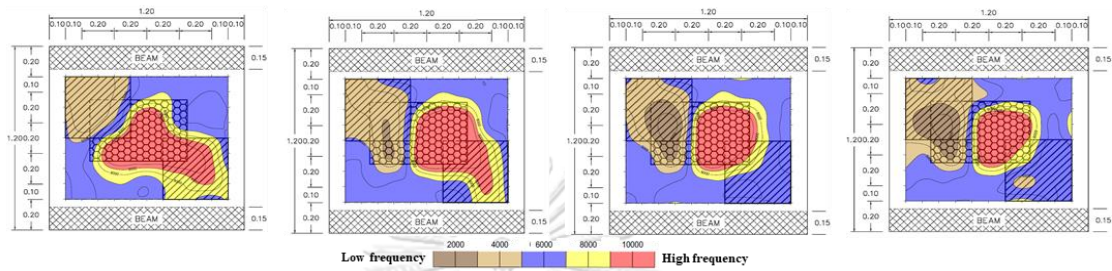
Then, the comparison of all grid-point testing methods from mock-up no.03 show that the IE method was more successfully detected simulated delamination and air-filled voids than the UPV method again. Only UPE contour map can show all simulated defects in this idealized structure; however, the IE and GPR contour map cannot show the deep simulated defects. The reason why almost equipments based NDT method cannot detect the deepest one is too thin layers at lower level of rebars and too weak detected signal. In conclusion, the ability of defect detection of any NDT methods on the mock-up no.03 can be orderly accuracy, precision, and performance by  $UPE > IE = GPR > UPV$  methods along the hardening period.

Last but not least, the comparison of all NDT results from mock-up no.04 was exhibited that the simulated unconsolidated concrete was not successfully detected over the hardening period by all equipments based on NDT method because they were maybe too small void and concrete ratio and the limitation of equipment. Thus, the limitation of all NDT methods in this idealized part is unconsolidated concrete or honeycomb. In conclusion, the ability of defect detection of all NDT methods on the mock-up no.04 can be concluded that accuracy, precision, and performance of all NDT methods are equal along the hardening period.

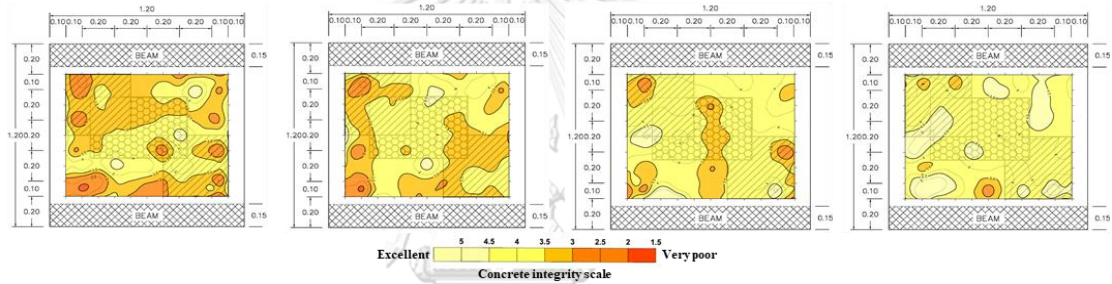
**A) Ultrasonic Pulse Echo Contour Maps**



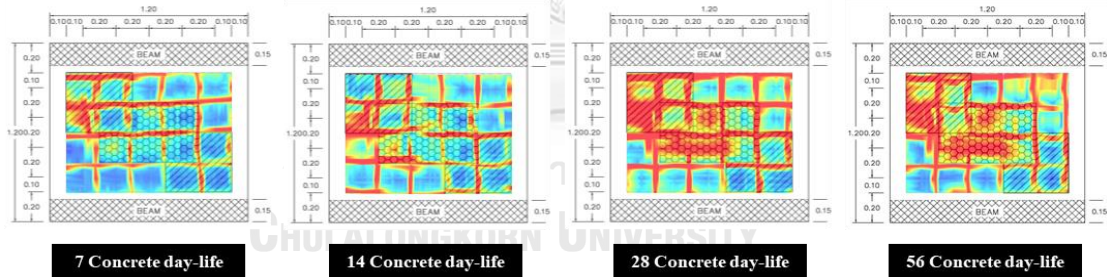
**B) Impact Echo Contour Maps**



**C) Ultrasonic Pulse Velocity Contour Maps**



**D) Ground Penetrating Radar Contour Maps**



7 Concrete day-life

14 Concrete day-life

28 Concrete day-life

56 Concrete day-life

Figure 39. All NDT contour maps of mock-up no.03 were illustrated over hardening period.



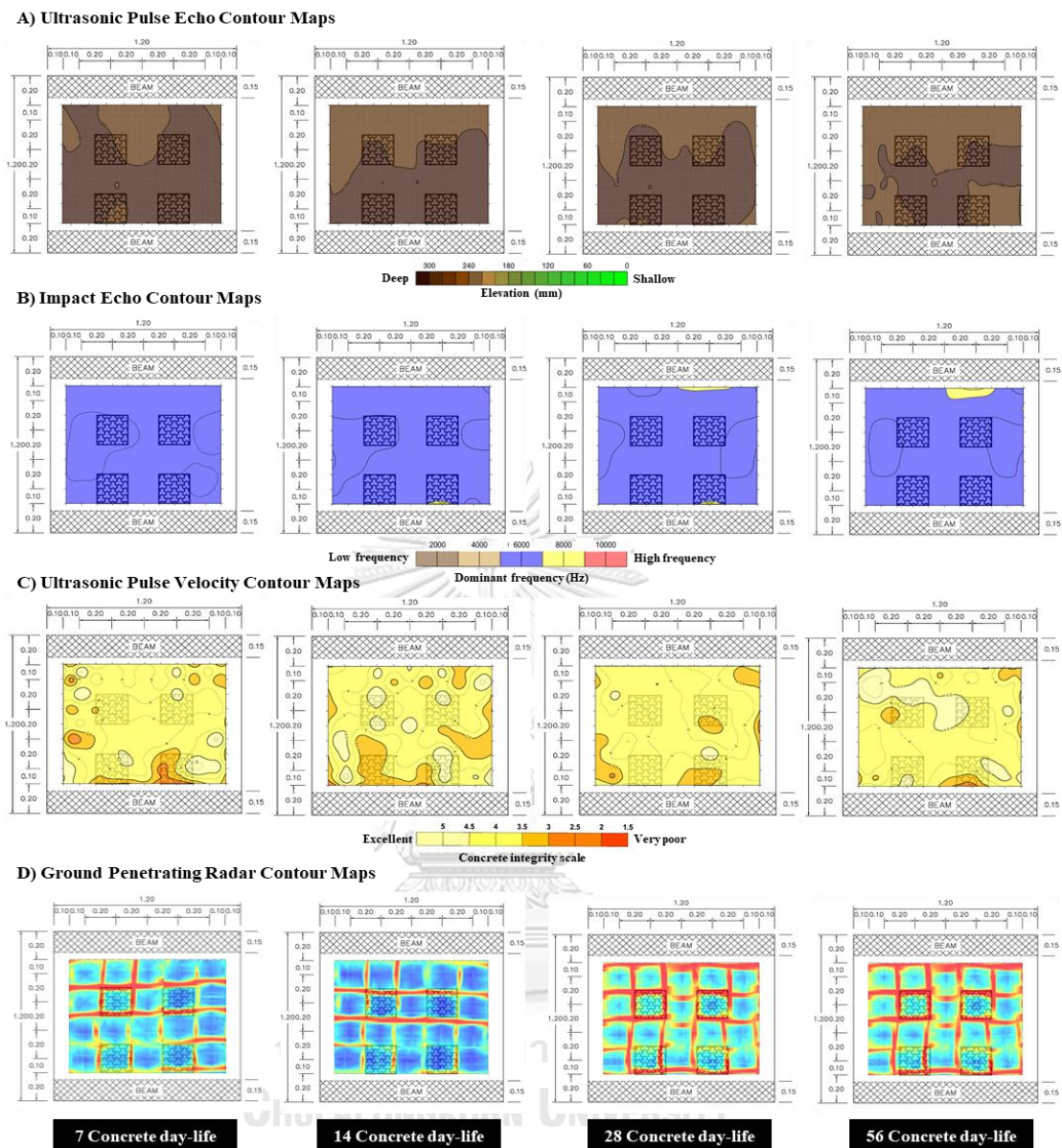


Figure 40. All NDT contour maps of mock-up no.04 were illustrated over hardening period.

The defect detectable results of four mock-ups simulated defects were accumulated and concluded in Table 5 below. The similar result is the UPV method is not succeeded in terms of defect detectability over the hardening period, while other NDT methods can. Therefore, the ability of defect detection of any NDT methods at the idealized structure can be orderly accuracy, precision, and performance by UPE > IE > GPR > UPV methods along the hardening period.

Table 5. The detectability of NDT methods over the hardening period were concluded from four RC mock-ups.

Mock-up name	Defect number	Defect dimension (mm)	Defect depth (mm)	Detectability of defect			
				GPR	UPE	IE	UPV
Delamination	No. 01	200x200	40.00	YES	YES	YES	NO
	No. 02	200x200	30.00	YES	YES	YES	NO
	No. 03	200x200	40.00	NO	YES	YES	NO
	No. 04	200x200	30.00	NO	YES	YES	NO
	No. 05	200x200	220.00	NO	NO	NO	NO
	No. 06	200x200	250.00	NO	YES	YES	NO
	No. 07	200x200	220.00	NO	YES	YES	NO
	No. 08	200x200	250.00	NO	YES	YES	NO
	No. 09	200x200	220.00	NO	YES	YES	NO
Air-filled void	No. 01	200x200	110.00	YES	YES	YES	NO
	No. 02	200x200	90.00	YES	YES	YES	NO
	No. 03	150x150	150.00	NO	NO	NO	NO
	No. 04	150x400	200.00	NO	NO	NO	NO
	No. 05	200x200	70.00	YES	YES	YES	NO
	No. 06	200x300	100.00	YES	YES	YES	NO
Delamination & air-filled void	No. 01	200x400	60.00	YES	YES	YES	NO
	No. 02	200x400	40.00	YES	YES	YES	NO
	No. 03	400x600	120.00 to 180.00	YES	YES	YES	NO
	No. 04	200x400	270.00	NO	YES	NO	NO
	No. 05	200x400	250.00	NO	YES	NO	NO
Unconsolidated concrete	No. 01	200x200	190.00	NO	NO	NO	NO
	No. 02	200x200	190.00	NO	NO	NO	NO
	No. 03	200x200	190.00	NO	NO	NO	NO
	No. 04	200x200	190.00	NO	NO	NO	NO

### 4.3 Realistic Structure in Research

The realistic structure in the research is an old warehouse somewhere in Bangkok, Thailand as shown in Figure 41 because a lot of crack lines were observed in the researching area as shown on a 1<sup>st</sup> floor plan in Figure 42. The background of the researching area was a warehouse that installed many large machines for production lines, thus the 1<sup>st</sup> floor slab detail was designed two layers consist of lean concrete thick 0.10 to 0.15 m below and cover with reinforcement concrete slab thick 0.10 m for supporting them as shown in Figure 44. However, the crack lines and any damages were many found by naked eyes on the overall realistic structure.



Figure 41. Overall realistic structure was inspected flaws in the research.

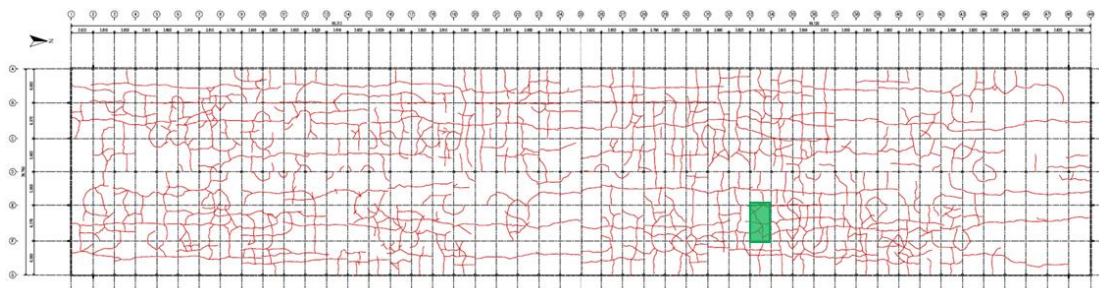


Figure 42. 1<sup>st</sup> floor plan illustrates crack lines (red) and a testing area (green).

Due to the warehouse is a very large area, approximately 36.78x198.00 m, thus only a selected small area, 3.00x3.00 m, was performed as shown in a green area or

gridline E-F/33-34 in Figure 42. The crack lines are illustrated in the researching area have approximate crack width from 0.35 to 0.80 mm which were randomly measured by crack scale ruler as shown in Figure 43. Moreover, the hammer sounding results on the researching area were shown ringing sound, red dot, at the almost area, which means two layers of slabs were separated together which maybe caused the crack lines or other damaged will be occurred in the future as shown in Figure 44.

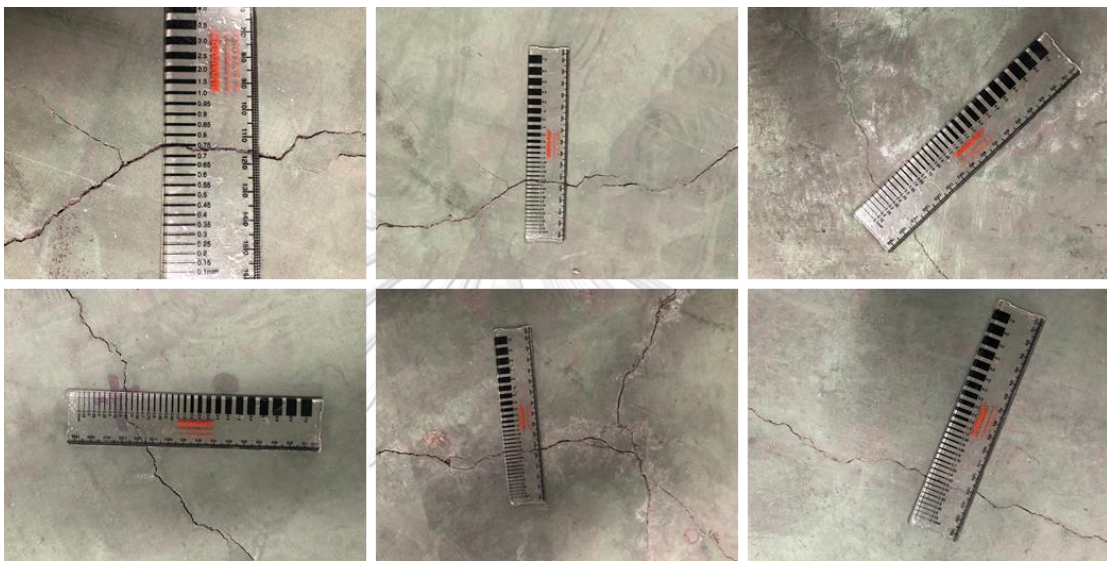


Figure 43. Example of crack width measurement was acquired by crack scale ruler on researching area.

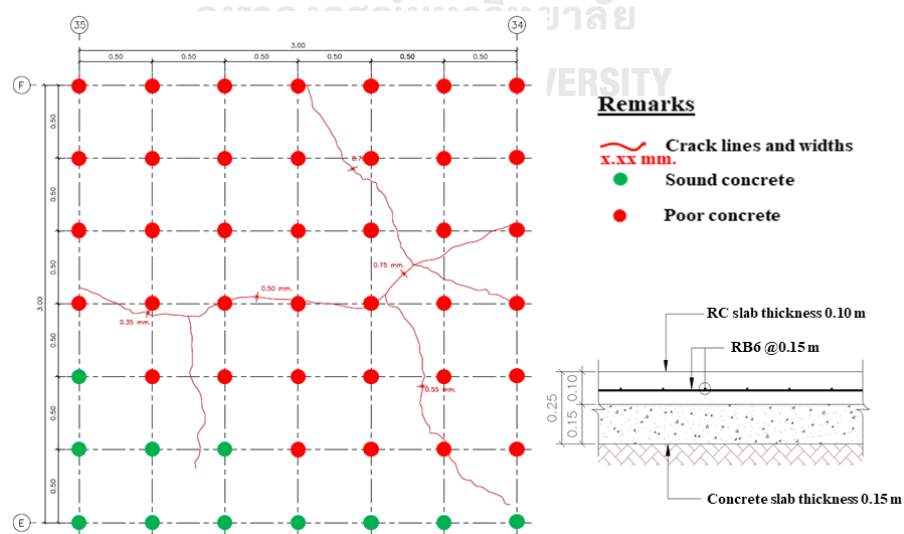


Figure 44. Visual inspection and hammer sounding were performed on researching area and sectional detail of RC slab was illustrated.

#### 4.4 Results of NDT signals on the Realistic Structure

The NDT methods on the realistic structure were performed as same as the previous section. However, the realistic structure is larger than the RC mock-ups, the testing patterns were adjusted for suitable acquisition related to the size of the structure or testing area. Then, the grid-point testing pattern has changed the spacing from 0.20 m to 0.50 m and the line-scan testing pattern, only the UPE method, was changed from 0.20 m to 0.50 m. The GPR method was only performed as same as the previous section because the function on the application was forced to acquire data in an image scan, 0.60x0.60 m. Figures 45 and 46 show the change of testing patterns on all NDT methods.

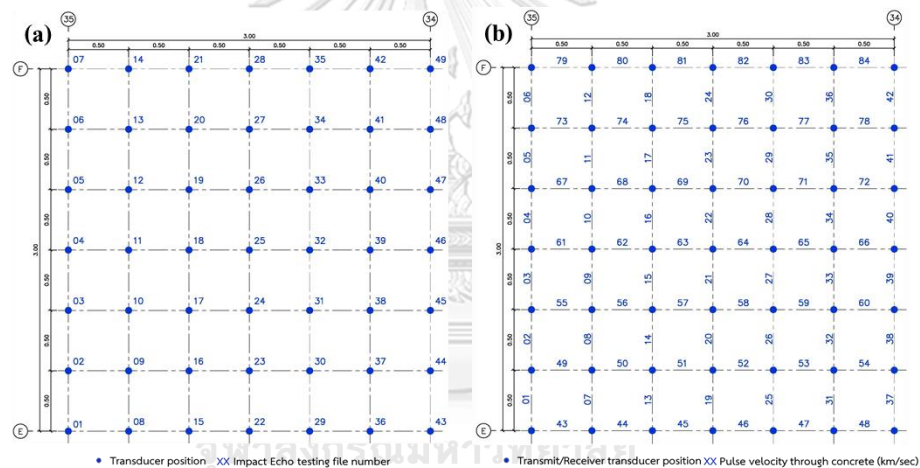


Figure 45. Plan view show testing patterns of a) IE and b) UPV methods.

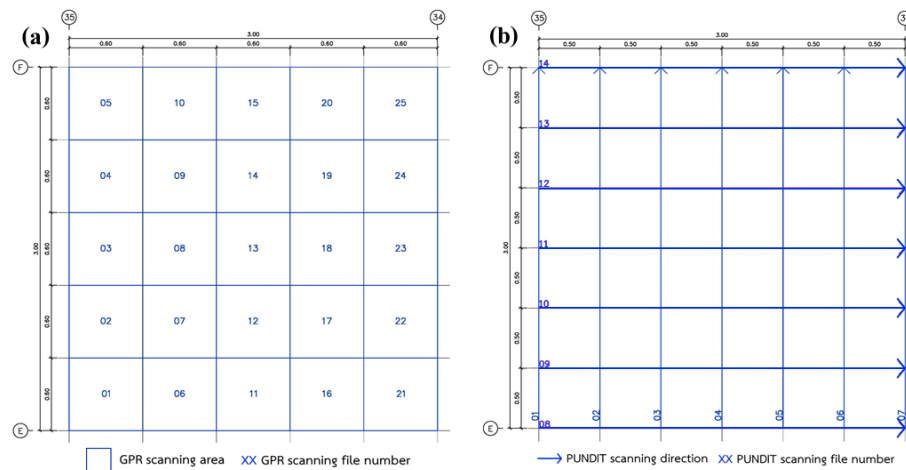
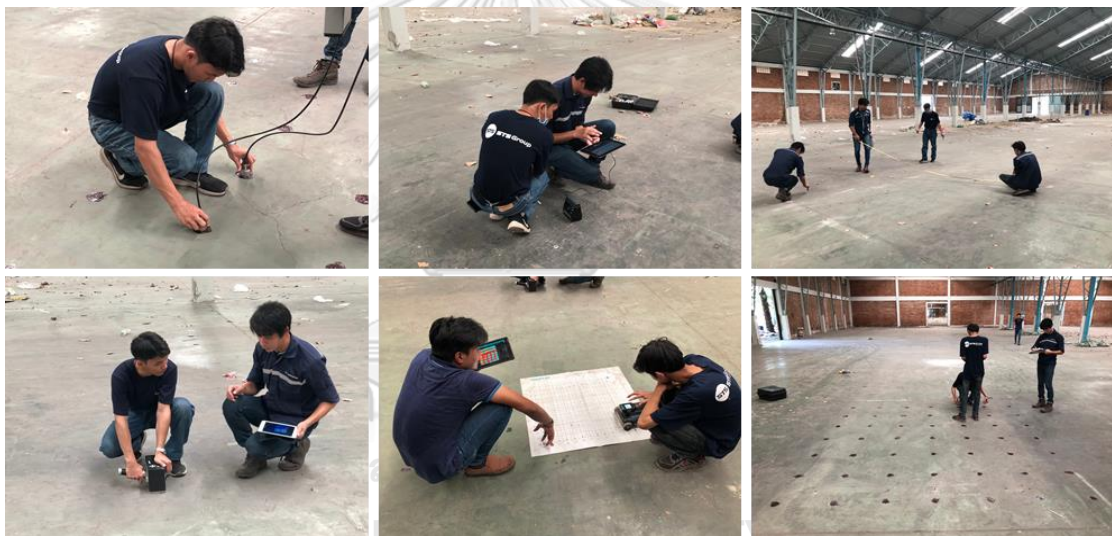


Figure 46. Plan view show testing patterns of a) GPR and b) UPE methods.

Then, the suitable parameters of the four NDT methods were calibrated with known concrete thickness of upper-part slab from the structure background. Firstly, the dielectric constant parameter of the GPR method was used values at 6.6 due to an old concrete day-life. Secondary, the shear-wave velocity values of the UPE method are approximately used valued at 2,500 m/s. Thirdly, the compressional-wave velocity values of the IE method are approximately used valued at 3,711 m/s. Finally, the UPV method was calibrated itself and the results were a relative comparison between point to point and were shown in concrete integrity range. The results from all NDT methods were generated contour maps for comparing together as same as previous part as shown in Figure 48 below.



**Figure 47. Four NDT method were performed on a testing area.**

The overall results on a researching area as shown in Figure 48 indicated that the concrete integrity in the researching area was a doubtful level from the appraisal of the UPV method. However, the other stress-wave based NDT method and the GPR results were found some anomalies which may be significant defects related to the researching objects. Therefore, the results of the researching area were randomly rechecked the suitability, accuracy, and precision by four coring positions as shown in Figure 48 , whereas any randomly coring positions were selected for different purposes. The purposes of the first position are to recheck the concrete integrity and

the missing of GPR signals as shown in the green rectangular in Figure 49a due to moisture or corroded rebar occurrence which can lead to delamination occurrence. The purposes of the second and fourth positions were an inspection of the significant detection of all the NDT methods which can be defects in this researching area. The profile comparisons between the GPR and UPE methods at the coring position number 02 and 04 were displayed in Figure 50 and 52. The purposes of another position are to confirm the thickness and quality of concrete as shown in Figure 51.

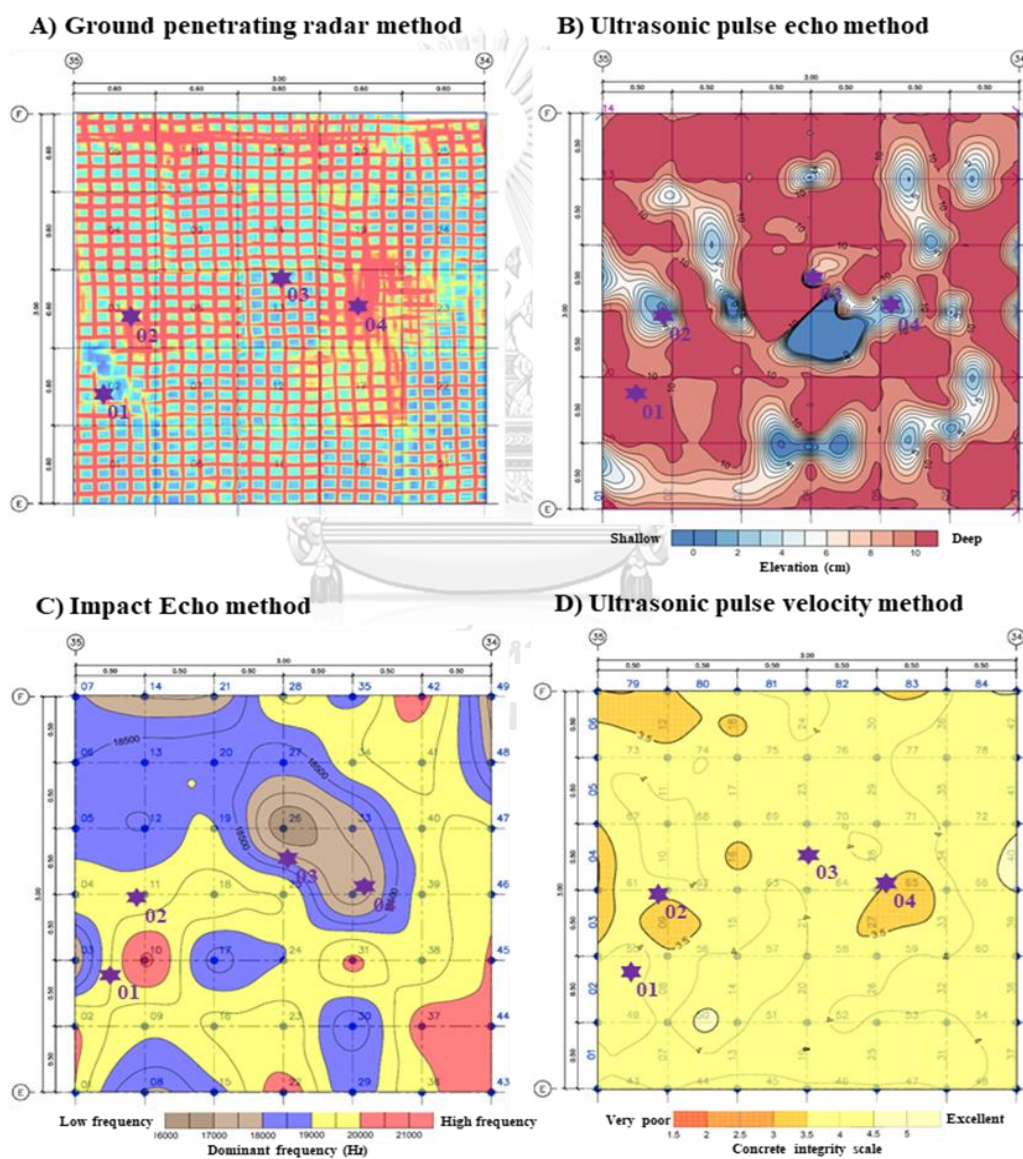


Figure 48. All NDT contour maps with selected coring positions (purple star) were illustrated on researching area.

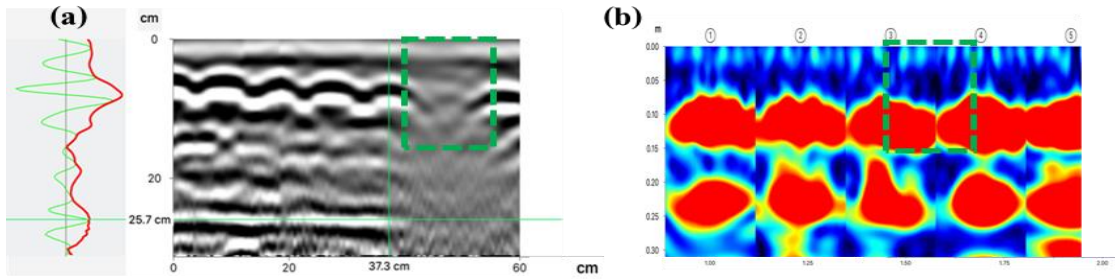


Figure 49. Comparison between a) GPR and b) UPE profiles were only shown missing signal (green rectangular) on GPR profile at coring position no.01.

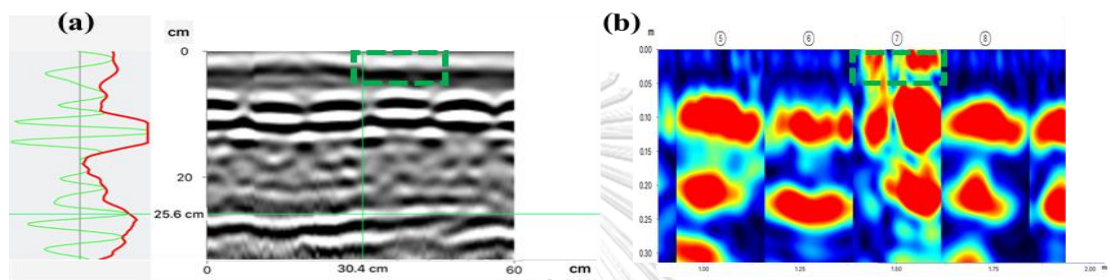


Figure 50. Comparison between a) GPR and b) UPE profiles were shown significant signal (green rectangular) on UPE profile at coring position no.02.

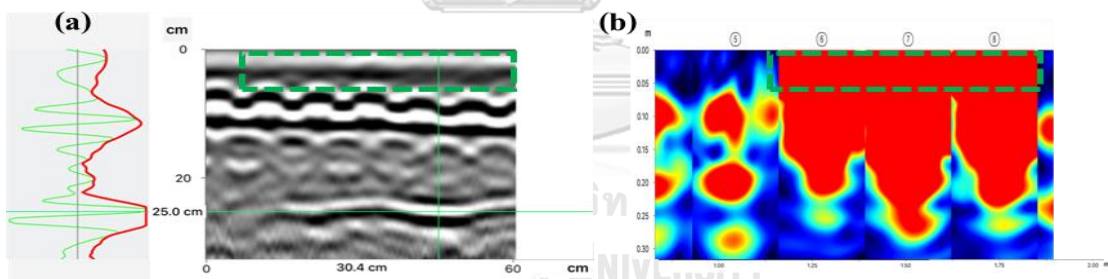


Figure 51. Comparison between a) GPR and b) UPE profiles were shown significant signal (green rectangular) on UPE profile at coring position no.03.

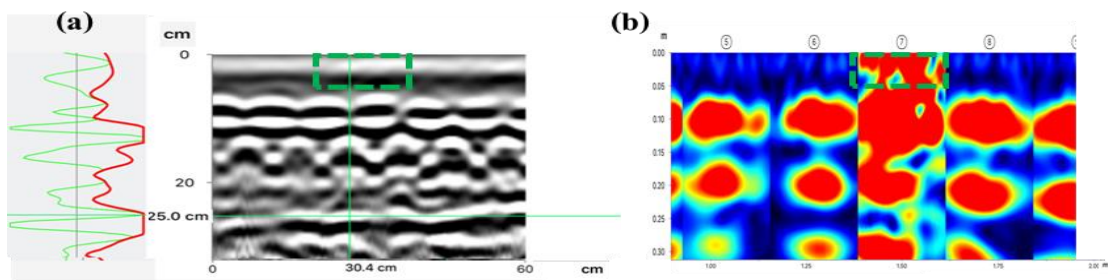


Figure 52. Comparison between a) GPR and b) UPE profiles were shown significant signal (green rectangular) on UPE profile at coring position no.04.



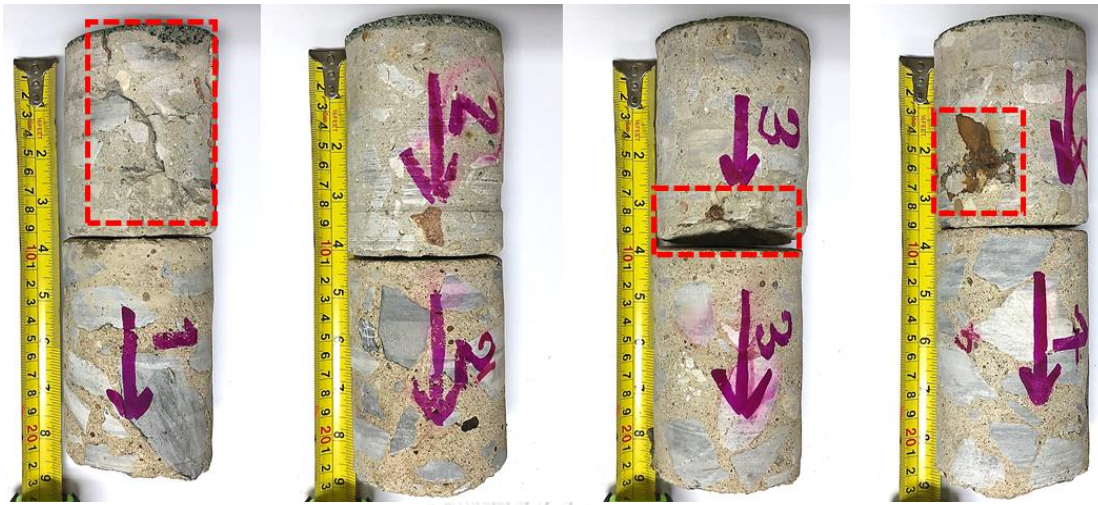


Figure 53. Four concrete coring samples were shown concrete integrity and physical defects (red rectangle).

Almost the randomly concrete cores were found differences of defects which were following described. First, the coring sample no.01 was displayed a lot of crack lines that were laid perpendicular with the concrete surface until the bottom of the upper part of RC slab and corroded rebar was found around the bottom of slab. Moreover, this position is the only one that was detected by the missing of GPR signal. However, the concrete integrity is classified in a good level. Second, the coring sample no.02 was not found any defects; moreover, the concrete integrity is classified in quite good level which was related with the UPV result. It was actually related with all NDT methods exclude the UPE method. The reason why only the UPE method is shown high reflection coefficient is caused from cupping, one type of error from acquisition which occurred when acquiring sensors were not completely attached with the testing surface. Then, the coring sample no.03 was found concrete spalling and corroded rebar exposed around the bottom of the upper part of RC slab. The physical damages as shown on it are the reason why very high reflection coefficient was distinguished by the UPE method is thin airgap, approximate width 1.00 to 2.00 cm, between two layers of slabs. However, the concrete integrity is classified in a good level which was related with the UPV result. Finally, the coring

sample no.04 was not found any defects; however, the rust aggregates were found a little bit which may be caused by nearby corroded rebar occurrence. Therefore, the concrete integrity of the last coring sample is classified in doubtful level which related with the UPV method and related with shallow reflection of the UPE and IE methods, respectively. Last but not least, Table 6 and Figure 53 are concluded the concrete coring results of any positions were compared with the four equipments based on NDT methods.

**Table 6. The detectability of NDT methods was descriptively compared with concrete cores.**

Coring No.	Non-destructive testing method				Concrete core detail
	GPR	UPV	UPE	IE	
No.01	Found anomaly	Good quality	Thick reflection	High frequency	<ul style="list-style-type: none"> <li>- Vertical crack lines are found along the coring thickness.</li> <li>- Corroded rebar are found around the bottom slab.</li> <li>- Concrete integrity is good level.</li> </ul>
No.02	Not found	Good quality	Shallow reflection	High frequency	<ul style="list-style-type: none"> <li>- Any defects and corroded rebar are not found.</li> <li>- Concrete integrity is good level.</li> </ul>
No.03	Not found	Good quality	Deep reflection	Low frequency	<ul style="list-style-type: none"> <li>- Thin air gap is found around the bottom slab.</li> <li>- Corroded rebar are found around the bottom slab</li> <li>- Concrete integrity is good level.</li> </ul>
No.04	Not found	Doubtful quality	Shallow reflection	Low frequency	<ul style="list-style-type: none"> <li>- Any defects and corroded rebar are not found.</li> <li>- Concrete integrity is doubtful level due to rust aggregates are found.</li> </ul>

## CHAPTER 5 DISCUSSIONS AND CONCLUSIONS

### 5.1 Discussions

Both visual inspection and hammer sounding methods are generally performed refer from ASTM standard as previously described on chapter 2. Both results based on visual inspection and hammer sounding from the realistic structure can be previously located the area which maybe have the delamination or/and air-filled void in the concrete structure. The advantages of both methods were saved cost and time to inspect; nevertheless, they were widely estimated the trouble area which maybe have or have not some defects. Thus, the abilities of four NDT methods which the researcher focused i.e., UPV, IE, UPE, and GPR methods are better than both visual inspection and hammer sounding methods because they were inspected by using the difference of material properties such as dielectric constant, elastic modulus, acoustic impedance, etc.

Four equipments based on NDT methods in this research have widely used the ability to inspect or detect the concrete integrity for long time ago; however, recent researches about concrete integrity were always compared between two NDT methods. Thus, this research is created with willing to compare the ability of defect inspection by four NDT methods. For this reason, all NDT results from both idealized structures and realistic structure in this research are discussed with the other related topics and researches, respectively.

The UPV method is possible to determine concrete uniformity included internal flaws and voids by grid point testing; however, UPV mapping results from the other previous researches have clearly concrete integrity criteria yet (Lorenzi et al., 2015) as shown the example velocity mappings in Figure 54 below. Therefore, this research is additionally contained the standard of concrete quality classification (Khan, 2002). The UPV mapping results in this research can be compared to other methods with higher accuracy and precision than the other previous research as shown in Figure 55.

However, the UPV results from both idealized structures and the realistic structure cannot indicate the levels and dimensions of defects like other NDT methods in this research can be due to the testing pattern and the limitation of this method. Although the testing pattern, indirect transmission pattern, is changed, the lasted results are still be the same which cannot show like other NDT methods.

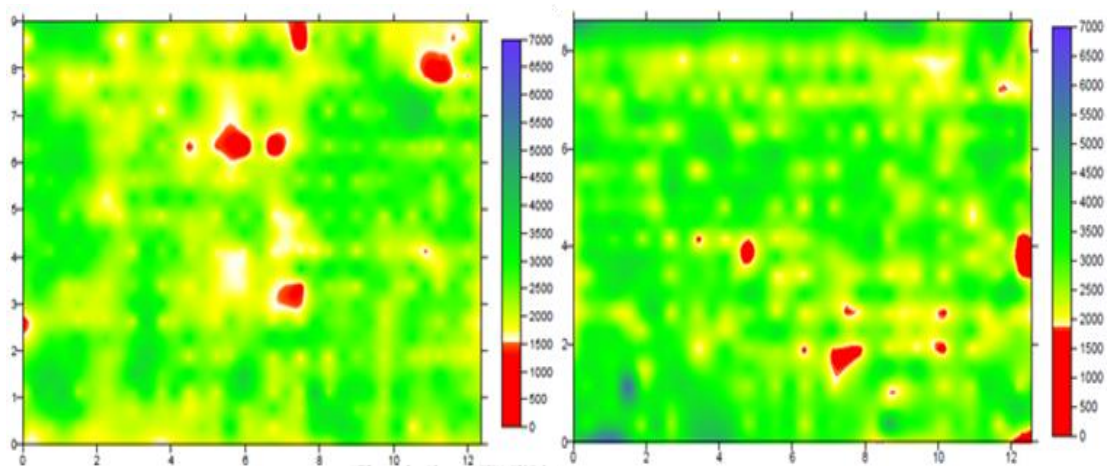


Figure 54. UPV contour mappings from other research were illustrated the difference using of concrete quality criteria (Lorenzi et al., 2015).

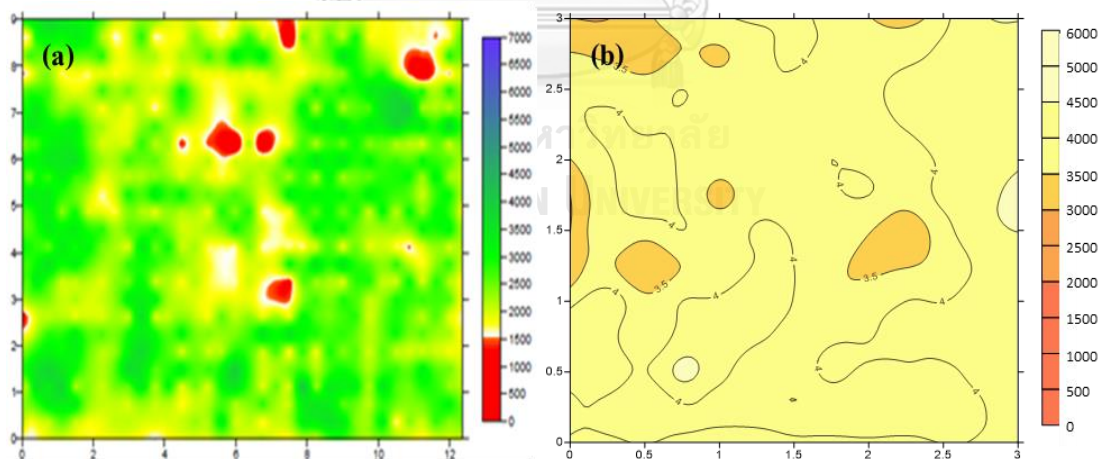


Figure 55. UPV contour mapping results between a) other research and b) this research were compared.

The IE method was possible to determine concrete uniformity like the other NDT methods; on the other hand, IE mapping results have not standard which indicate

the level and position of defects. The international criteria of this methods must firstly find the suitable P-wave velocity or thickness frequency which depend upon the structure thickness (Azari et al., 2014) as shown in Figure 56. Owing to, the dominant frequency decreases as the structure thickness increases as shown in Figure 57 because of less energy reflected to the recorder. Thus, the peak frequency that out the range of the thickness frequency is possible to be defects. Furthermore, the signal characteristics of the peak frequency can be approximately used to indicate the dimension, depth, and thickness that was required more technical experience than the UPV method. The research results was related to the other previous researches as shown in Figure 58.

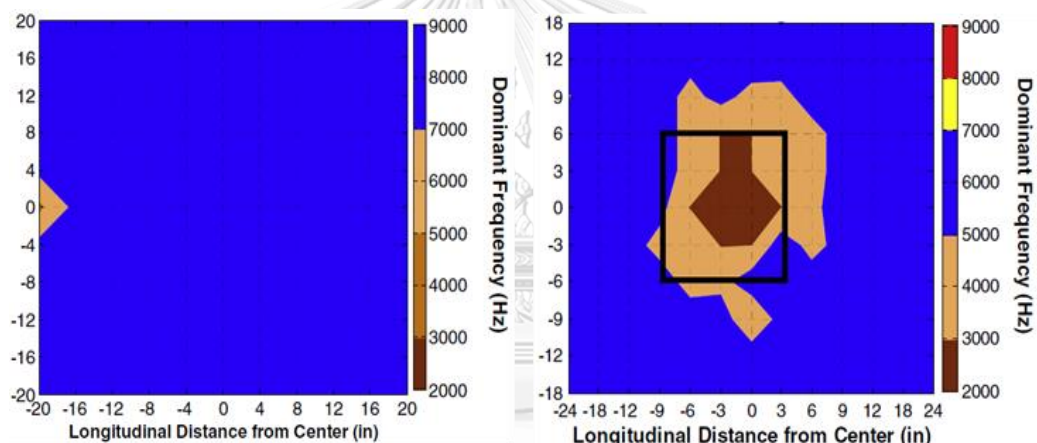


Figure 56. IE contour mappings from other research were illustrated the differentt using of dominant criteria (Azari et al., 2014).

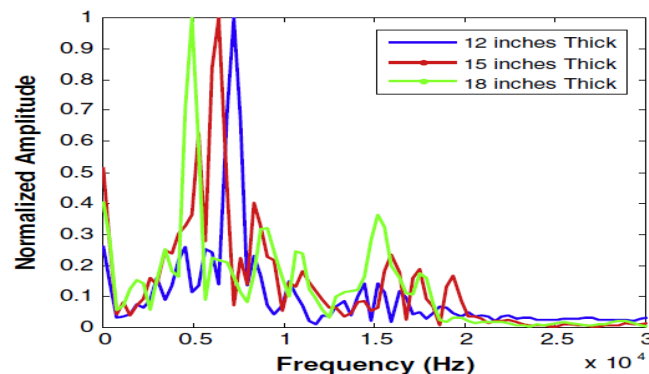


Figure 57. Different concrete thickness affect to dominant frequency (Azari et al., 2014).

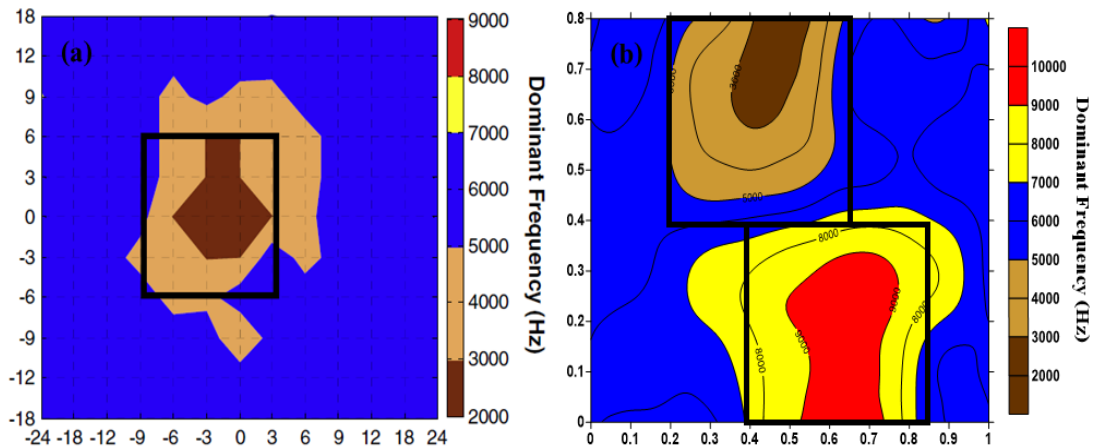


Figure 58. IE contour mapping results between a) other research and b) this research were compared.

In addition, the IE results from both idealized structures and the realistic structure can locate the different levels of defects. Although the concrete day-life is early age, this signal results are still inspected them along the hardening period. Nevertheless, the precision and accuracy of defect dimension are dependent on software generating.

The UPE method is widely used to inspect flaws and thickness along concrete pavement by Department of Transportation, USA because this technique is friendly used and not required much of technical experiences. Thus, the change of signal characteristic is the criteria of flaw detection which can locate the level and dimension of the defects (Stefan et al., 2018). The international criteria of this methods must firstly find the suitable S-wave velocity which depend upon the structure thickness. Consequently, the results are shown the reflected level along sectional-profiles due to the reflection coefficient or energy is affected to the signal characteristic as shown in Figure 59 below. The results of this research are related with the other previous researches which was reflected at the dissimilar layers as shown in Figure 28 to 31 and 50 to 52 of the idealized structures and the realistic structure, respectively. Furthermore, the UPE results from both idealized structures and the realistic structure can locate the different levels and dimensions of defects,

while the concrete day-life is still early age. Nevertheless, the results of other researches are often shown and discussed by sectional profiles. The results of this research is additionally illustrated in the form of contour maps represented the reflected level as shown in Figure 60 for easily comparing with the other methods.

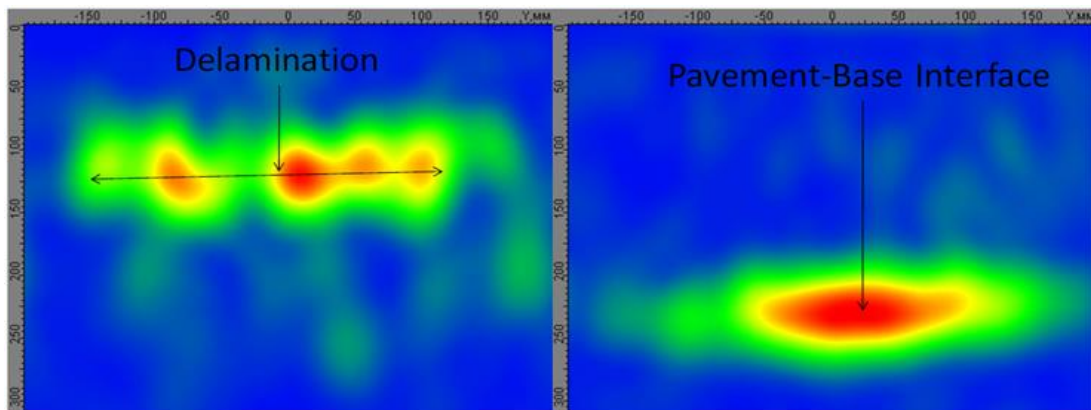


Figure 59. Example of UPE profiles show the profile results over delamination (left) and sound concrete (right) (Stefan et al., 2018).

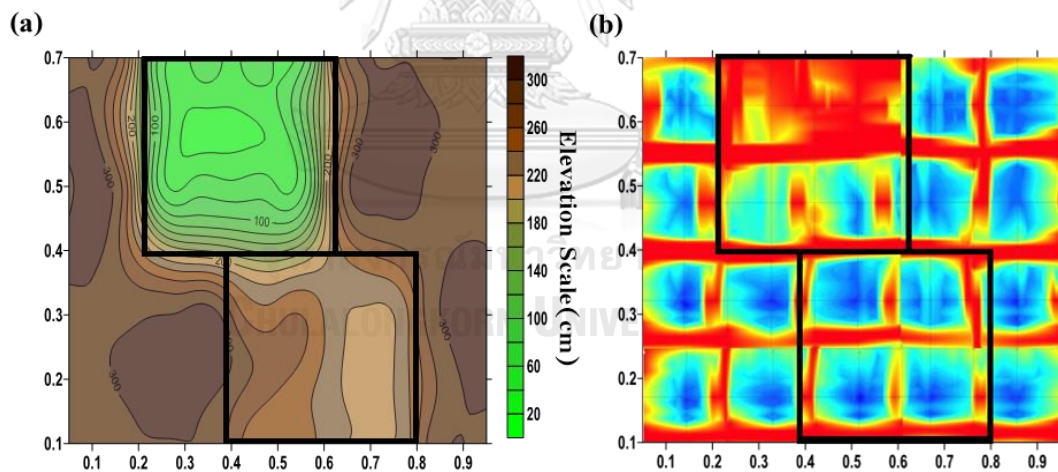


Figure 60. Example research result of a) UPE and b) GPR were illustrated by contour map.

The GPR method is successfully detected centimeter to meter scale of underground water and air-filled void in geotechnical term but the defects in the RC building were still needed further researches. The equipment frequency in civil engineering work is higher than the other types of work that exhibit the higher

resolution too (Venkateswarlu & Tewari, 2014); however, the GPR method is quietly sensitive to steel or metallic materials which hardly inspected the defects. Furthermore, the previous researches about composite peak amplitude of the superimposed wavelets (David, 2017) were concluded that the superposition of the reflection at top and bottom of the void yields a peak amplitude that is almost fifty percentage greater than the amplitude of a single reflection. However, they are not always present. Owing to, the using of higher frequency decrease the reflection of void thickness peak response as shown in Figure 61. The researching results from both idealized structures and the realistic structure are related with the other field of researches i.e. geotechnical engineering, and geology which is reflected at the dissimilar layers; however, other research results are more difficult to interpret than RC structures because they have the structural pattern which can easily identify the defects as shown in Figure 61.

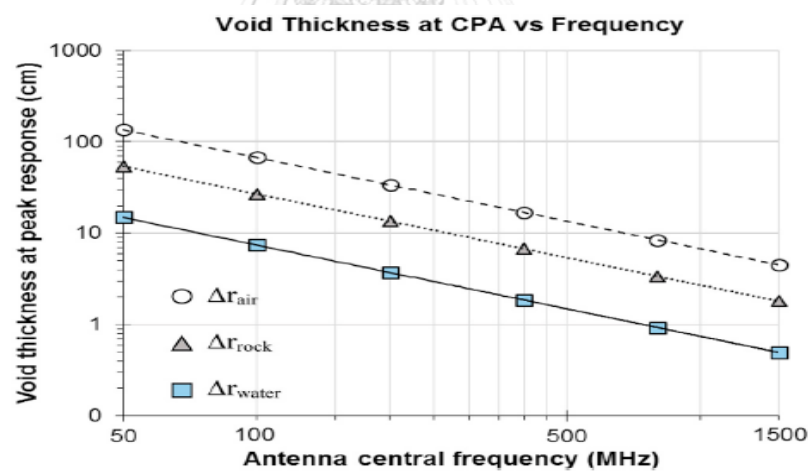


Figure 61. Void thickness at the peak response as a function of material and frequency (David, 2017).

Moreover, if defects in RC structures are larger enough and the position is not closed to the rebars or metallic materials and structural thickness, it is the successful NDT method which has the ability to locate and scope the deflection in concrete. However, this method is required to perform at aging concrete, older than the hardening period, owing to the results are higher resolution to detect them.



From the previous comparisons with other literatures, almost four equipments based on NDT methods successfully locate variety of defects within the concrete elements consisting of delamination, and voids except honeycombing in this research. To summarize the objectives of this research, the performance, suitability, accuracy, and precision for detecting size, shape, position, and level of simulated defects of idealized structures over the hardening period and the realistic structure of each techniques are concluded and ranked in Table 7 below.

**Table 7. Summary of Descriptive comparison of ranked lists. The detectability of NDT methods were descriptively compared with concrete cores.**

Device	Accuracy & Precision	Suitability	Performance	Ranking
UPE	High accuracy and high precision because it can clearly locate and scope the defect on both structures	Suitable with every sizes and shapes of testing areas or structures with all concrete age	High performance to detect and display all levels and dimensions of the defect	1
GPR	Moderate accuracy but high precision because it can clearly locate and scope the defect on both structures	Suitable with every sizes and shapes of testing areas or structures with old concrete age, older than hardening peroid	Moderate to high performance to detect and display all levels and dimensions of the defect	2
IE	High accuracy but moderate precision due to it can locate and scope the defect on both structures	Suitable with every sizes and shapes of testing areas or structures with all concrete age	Moderate performance to detect all levels and dimensions of of the defect	3
UPV	Low accuracy and precision due to it cannot locate and scope the defect on both structures	Suitable with every sizes and shapes of testing areas or structures with all concrete age	Low performance to detect and display all levels and dimensions of of the defect	4

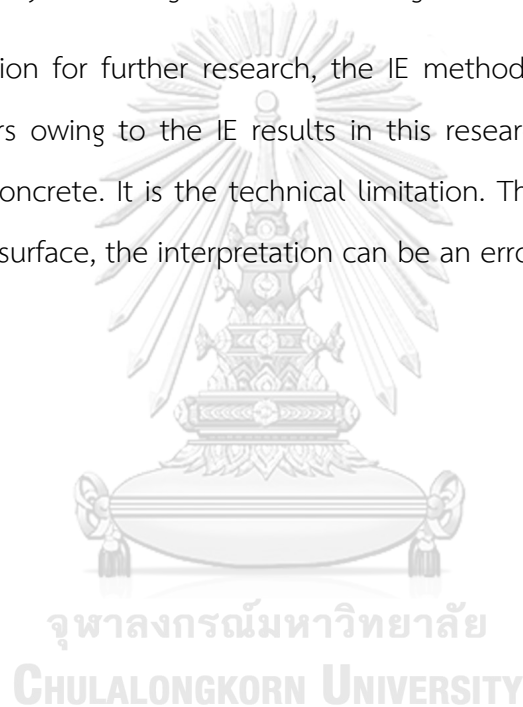
## 5.2 Conclusions

Almost four equipments based on NDT methods in this research were performed very well in locating the simulated delamination and air-filled voids, over the hardening period except for the UPV method which only show concrete integrity on the testing area. The UPV method is not successful to indicate the difference of defect levels and dimensions in both parts of this research because of the limitation of this UPV method which only represent the integrity of concrete between two transducers. However, the UPV method, one of stress wave-based NDT method, can performed at every concrete day-life, the GPR method cannot. The difference of concrete day-life only affected the GPR method because the resolution for locating defects and thickness was dependent on the dielectric constant of materials which were sensitive to water content in the concrete. Moreover, the limitation of the GPR method was that it cannot obviously illustrate deep defects close-up with the opposite side of the structure due to the weak reflection signals that can be merged with thickness reflection. On the other hand, the UPE and IE methods can successfully be located all levels of defects and concrete thickness over the hardening period, but only the UPE results can be represented the continuous reflection level and scoping area in both cross-sectional profiles and contour map. In conclusion, the ranking of any NDT methods in the idealized structure part refer from Table 5 can be orderly accuracy, precision, and performance by the UPE method, the IE method, the GPR method, and the UPV method, respectively.

On the contrary, the realistic structures that researcher's experiences were often performed on the aging structure longer than 58 days, as same as the researching area, except for the accident from the construction processes, such as too fast to release concrete mold, concrete explode from release stressing tendon, etc. Thus, the GPR method has performance to detect and then exhibit the delamination and air-filled voids in the aging concrete too. In addition, the duration of data acquisition and data interpretation of the GPR method is similar as the UPE method which save

time than the other methods and illustrate the continuous results. In conclusion, the ranking of any NDT methods in both parts, perform on idealized structures and the realistic structure, refer from Table 7 can be orderly accuracy, precision, and performance by the UPE method, the GPR method, the IE method, and the UPV method, respectively. Consequently, the researcher suggested that the GPR and UPE methods should be performed together for higher accuracy and precision of the results while testing the unknown deflection. Furthermore, the results should be randomly checked by the coring method for saving cost and time at remedy process.

Recommendation for further research, the IE method should be performed by air-coupled sensors owing to the IE results in this research were not acquired the shallow level of concrete. It is the technical limitation. Thus, if the defects are very close up with the surface, the interpretation can be an error from missing the data.



## REFERENCES

- ACI. (1998). Nondestructive Test Methods for Evaluation of concrete in structure. In (Vol. ACI 228.2 R). USA: Farmington Hills.
- ACI. (2008). Guide for conducting a visual inspection of concrete in service. In (Vol. ACI 201.1 R). USA: Farmington Hills.
- Andrzej, M., & Marta, M. (2014). Modern NDT Systems for Structural Integrity Examination of Concrete Bridge Structures. *Procedia Engineering*(91), 418-423.  
doi:10.1016/j.proeng.2014.12.086
- ASTM. (1998). Standard test method for measuring the P-wave speed and the thickness of concrete plates using the impact-echo method. In (Vol. ASTM C-1383). West Conshohocken: American Society for Testing and Materials.
- ASTM. (2002). Standard test method for pulse velocity through concrete. In (Vol. ASTM C597). West Conshohocken: American Society for Testing and Materials.
- ASTM. (2003). Standard practice for measuring delaminations in concrete bridge decks by sounding. In (Vol. ASTM D4580-03). West Conshohocken: American Society for Testing and Materials.
- ASTM. (2010). Standard Test Method for Determining the Thickness of Bound Pavement Layers Using Short-Pulse Radar. In (Vol. ASTM D4748). West Conshohocken: American Society for Testing and Materials.
- Azari, H., Nazarian, S., & Yuan, D. (2014). Assessing sensitivity of impact echo and ultrasonic surface waves methods for nondestructive evaluation of concrete structures. *Construction and Building Materials*, 71, 384-391.  
doi:10.1016/j.conbuildmat.2014.08.056
- Carino, N. J. (2015). *Impact Echo : The Fundamentals*. Paper presented at the International Symposium Non-Destructive Testing in Civil Engineering (NDT-CE) [https://www.ndt.net/article/ndtce2015/papers/257\\_carino\\_nicholas.pdf](https://www.ndt.net/article/ndtce2015/papers/257_carino_nicholas.pdf)
- Clausen, J., Zoidis, N., & Knudsen, A. (2012). Onsite measurements of concrete structures using Impact-Echo and Impulse Response. *Emerging Technologies in Non-Destructive Testing*, 5, 117-122. doi:10.1201/b11837-22

- Cusson, D., Lounis, Z., & Daigle, L. (2011). Durability Monitoring for Improved Service Life Predictions of Concrete Bridge Decks in Corrosive Environments. *Computer-Aided Civil and Infrastructure Engineering*, 26, 524-541. doi:10.1111/j.1467-8667.2010.00710.x
- David, C. N. (2017). Ground penetrating radar response from voids: A demonstration using a simple model. *NDT & E International*, 91, 47-53.
- Hoegh, K., Khazanovich, L., & Yu, H. T. (2011). Ultrasonic Tomography for Evaluation of Concrete Pavements. *Transportation Research Record: Journal of the Transportation Research Board*, 2232, 85-94. doi:10.3141/2232-09
- Jaw, S. W., & Hashim, M. (2013). Locational accuracy of underground utility mapping using ground penetrating radar. *Tunneling and Underground Space Technology*, 35, 20-29. doi:10.1016/j.tust.2012.11.007
- Kaplanvural, I., Pekşen, E., & Özkap, K. (2018). Volumetric water content estimation of C-30 concrete using GPR. *Construction and Building Materials*, 166. doi:10.1016/j.conbuildmat.2018.01.132
- Karaiskos, G., Deraemaeker, A., Aggelis, D. G., & Hemelrijck, D. V. (2015). Monitoring of concrete structures using the ultrasonic pulse velocity method. *Smart Materials and Structures*, 24. doi:10.1088/0964-1726/24/11/113001
- Khan, A. A. (2002). *Guidebook on non-destructive testing of concrete structures*. Vienna: International Atomic Energy Agency.
- Lai, W. W., Chang, R. K., & Sham, J. F. (2018). A blind test of nondestructive underground void detection by ground penetrating radar (GPR). *Journal of Applied Geophysics*, 149, 10-17. doi:10.1016/j.jappgeo.2017.12.010
- Landkard, D. L., Birkimer, D. L., Fondriest, F. F., & M.J., S. (1968). *The effects of moisture concrete on the construction and structural properties of portland cement concrete exposed to temperature up to 500 F.*  
<https://www.concrete.org/publications/internationalconcreteabstractsportal/m/details/id/17332>
- Lorenzi, A., Caetano, L. F., Campagnolo, J. L., Lorenzi, L. S., & Pinto da Silva Filho, L. C. (2015). Application of ultrasonic pulse velocity to detect concrete flaws. Retrieved from <https://www.ndt.net/article/ndtnet/2015/Lorenzi1.pdf>

- Lybeart, M. (2017). *Ultrasonic tomography, a non-destructive measuring technique for analysis of concrete roads*. Retrieved from Belgium:  
[https://ectri.org/static/YRS15/Documents/Papers&presentations/Session%20B%20Transport%20Civil%20&%20Road%20Engineering/Papers/Ultrasonic\\_tomography\\_a\\_non-destructive\\_measuring\\_technique\\_for\\_analysis\\_of\\_concrete\\_roads\\_LYBAERT.pdf](https://ectri.org/static/YRS15/Documents/Papers&presentations/Session%20B%20Transport%20Civil%20&%20Road%20Engineering/Papers/Ultrasonic_tomography_a_non-destructive_measuring_technique_for_analysis_of_concrete_roads_LYBAERT.pdf)
- Metwaly, M. (2015). Application of GPR technique for subsurface utility mapping: A case study from urban area of Holy Mecca, Saudi Arabia. *Measurement*, 60, 139-145. doi:10.1016/j.measurement.2014.09.064
- Meyer, K., Erdogmus, E., Morcou, G., & Naughtin, M. (2008). Use of Ground Penetrating Radar for Accurate Concrete Thickness Measurements. *Architectural Engineering Conference (AEI)*. doi:10.1061/41002(328)67
- Nguyen, L. T., & Modrak, R. T. (2018). Ultrasonic wavefield inversion and migration in complex heterogeneous structures: 2D numerical imaging and nondestructive testing experiments. *Ultrasonics*. 357-370. doi:10.1016/j.ultras.2017.09.011
- Oh, T., Kee, S., A., R. W., Popovics, J. S., & Zhu, J. (2013). Comparison of NDT Methods for Assessment of a Concrete Bridge Deck. *Journal of Engineering Mechanics*, 139, 305-314. doi:10.1061/(asce)em.1943-7889.0000441
- Richart, F., Hall, J., & Woods, R. (1970). *Vibrations of soils and foundations*. Prentice-Hall Inc.
- Sansalone, M., & Carino, N. J. (1991). Stress Wave Propagation Methods. In 5 (Ed.), *Handbook on Nondestructive Testing of Concrete*. Boca Raton, Florida: M. Malhotra and N.J. Carino, CRC Press.
- Sansalone, M. J., & Streett, W. B. (1997). *Impact-echo: Nondestructive evaluation of concrete and masonry*. Ithaca, N.Y: Bullbrier Press.
- Settrabut, C. (1997). Concrete Technology. In (pp. 143-153). Retrieved from <https://www.cpacacademy.com/index.php?tpid=0063>
- Stefan, M., Salvador, V., & David, S. (2018). Validation of artificial defects for Non-destructive testing measurements on a reference structure. *MATEC Web of Conferences*, 199(06006), 1-9. doi:10.1051/mateconf/201819906006
- Venkateswarlu, B., & Tewari, V. C. (2014). *Geotechnical applications of ground*

*penetrating radar (GPR)*. Paper presented at the Proceedings of the 15th International Conference on Ground Penetrating Radar.

Vonk, S., & Taffe, A. (2018). Detection of near-surface reinforcement in concrete components with ultrasound. *MATEC Web of Conferences*, 199(06007). doi:10.1051/mateconf/201819906007

Zoidis, N., Tatsis, E., Vlachopoulos, C., Gotzamanis, A., Clausen, J. S., Aggelis, D. G., & Matikas, T. E. (2013). Inspection, evaluation and repair monitoring of cracked concrete floor using NDT methods. *Construction and Building Materials*, 48, 1302-1308. doi:10.1016/j.conbuildmat.2013.06.082





จุฬาลงกรณ์มหาวิทยาลัย  
**CHULALONGKORN UNIVERSITY**



## VITA

**NAME** Thanakit Klomkliew

**DATE OF BIRTH** 9 May 1994

**PLACE OF BIRTH** Bangkok, Thailand

**INSTITUTIONS ATTENDED** Chulalongkorn university

**HOME ADDRESS**

**PUBLICATION**

- Fracture system of Khao Tham Hole, Changwat Phetchaburi
- Structural geology for estimate potential of solidified shale of Sap Bon formation at Amphoe Cha Lerm Phra Kit, Changwat Saraburi.

**AWARD RECEIVED** Excellent Internship Program 14th from SCG (Siam Cement Group)